

Validation of the Aura Microwave Limb Sounder CIO Measurements

M. L. Santee,¹ A. Lambert,¹ W. G. Read,¹ N. J. Livesey,¹ G. L. Manney,^{1,2} R. E. Cofield,¹
 D. T. Cuddy,¹ W. H. Daffer,¹ B. J. Drouin,¹ L. Froidevaux,¹ R. A. Fuller,¹ R. F. Jarnot,¹
 B. W. Knosp,¹ V. S. Perun,¹ W. V. Snyder,¹ P. C. Stek,¹ R. P. Thurstans,¹ P. A. Wagner,¹
 J. W. Waters,¹ J. Urban,³ D. Murtagh,³ P. Ricaud,⁴ B. Barret,⁴ A. Kleinböhl,¹
 J. Kuttippurath,^{5,6} H. Küllmann,⁵ M. von Hobe,⁷ G. C. Toon,¹ and R. A. Stachnik¹

¹ Short title: VALIDATION OF AURA MLS CLO DATA

¹Jet Propulsion Laboratory, California Institute of Technology, Pasadena, California, USA.

²Also at Department of Physics, New Mexico Institute of Mining and Technology, Socorro, New Mexico, USA.

³Department of Radio and Space Science, Chalmers University of Technology, Göteborg, Sweden.

⁴Laboratoire d'Aérodynamique, Observatoire de Midi-Pyrénées, Toulouse, France.

⁵Institute of Environmental Physics, University of Bremen, Bremen, Germany.

⁶Now at LMD/CNRS Ecole Polytechnique, Palaiseau, France.

⁷Institut für Chemie und Dynamik der Geosphäre I: Stratosphäre (ICG-I), Forschungszentrum Jülich, Jülich, Germany.

Abstract. We assess the quality of the version 2.2 (v2.2) ClO measurements from the Microwave Limb Sounder (MLS) on the Earth Observing System Aura satellite. The MLS v2.2 ClO data are scientifically useful over the range 100 to 1 hPa, with a single-profile precision of ~ 0.1 ppbv throughout most of the vertical domain. Vertical resolution is $\sim 3\text{--}4$ km. Comparisons with climatology and correlative measurements from a variety of different platforms indicate that both the amplitude and the altitude of the peak in the ClO profile in the upper stratosphere are well determined by MLS. The latitudinal and seasonal variations in the ClO distribution in the lower stratosphere are also well determined, but a substantial negative bias is present in both daytime and nighttime mixing ratios at retrieval levels below (i.e., pressures larger than) 22 hPa. In studies for which knowledge of lower stratospheric ClO mixing ratios to better than a few tenths of a ppbv is needed, it is recommended that this negative bias be corrected for by subtracting the estimated value of the bias from the individual measurements at each affected retrieval level.

1. Introduction

The partitioning between active and reservoir forms of chlorine modulates ozone destruction throughout the stratosphere [e.g., *Solomon, 1999; World Meteorological Organization, 2007*]. Chlorine monoxide, ClO, is the primary form of reactive chlorine in the stratosphere and thus a key catalyst for ozone loss. The Microwave Limb Sounder (MLS) on NASA's Earth Observing System (EOS) Aura satellite measures vertical profiles of ClO globally on a daily basis. Initial validation of the first publicly-available Aura MLS ClO dataset, version 1.5 (v1.5), was presented by *Barret et al. [2006]*. Here we report on the quality of the recently-released version 2.2 (v2.2) Aura MLS ClO measurements. The measurement system is described in section 2. In addition to providing a review of instrumental and orbital characteristics, this section includes guidelines for quality control that should be applied to the v2.2 ClO measurements, documents their precision and spatial resolution, and quantifies sources of systematic uncertainty. Because the v1.5 Aura MLS ClO data have been featured in some previous studies [e.g., *Schoeberl et al., 2006a; Santee et al., 2005*], section 2 provides an overview of the differences between v2.2 and v1.5 ClO data. A systematic negative bias, present in v1.5 but, unfortunately, worse in v2.2, is also quantified in this section. In section 3, 'zeroth-order' validation of the Aura MLS ClO data is accomplished by comparing against climatological averages in narrow equivalent-latitude bands compiled from the multi-year Upper Atmosphere Research Satellite (UARS) MLS ClO dataset. Accuracy is assessed through comparisons with correlative datasets from a variety of platforms in section 4. Finally, in section 5 we summarize the Aura MLS ClO validation results.

2. Aura MLS CIO Measurement Description

2.1. Overview of the MLS Measurement System

Aura, the last in NASA's EOS series of satellites, was launched on 15 July 2004 into a near-polar, sun-synchronous, 705-km altitude orbit with a 13:45 ascending equator-crossing time [Schoeberl *et al.*, 2006b]. One of its four instruments, Aura MLS, is an advanced successor to the Microwave Limb Sounder on UARS. Detailed information on the microwave limb sounding technique in general and the Aura MLS instrument in particular is given by Waters [1993] and Waters *et al.* [2006], respectively. MLS observes a large suite of atmospheric parameters by measuring millimeter- and submillimeter-wavelength thermal emission from Earth's limb with seven radiometers covering five broad spectral regions. The standard CIO product is retrieved from radiances measured by the radiometer centered near 640 GHz, which covers the strong CIO rotational line at 649.5 GHz. CIO is also measured by the 190-GHz radiometer (using the 204.4 GHz CIO line measured by UARS MLS), but these retrievals have slightly poorer precision and are not considered further here.

The Aura MLS fields-of-view point forward in the direction of orbital motion and vertically scan the limb in the orbit plane, leading to data coverage from 82°S to 82°N latitude on every orbit. Thus Aura MLS obtains continuous daily sampling of both polar regions, with none of the temporal gaps from yaw maneuvers that occurred with UARS MLS. The MLS limb scans are synchronized to the Aura orbit, with 240 scans per orbit at essentially fixed latitudes. This results in ~3500 scans per day, with an along-track separation between adjacent retrieved profiles of 1.5° great circle angle (~165 km). The longitudinal separation

of MLS measurements, set by the Aura orbit, is 10° – 20° over low and middle latitudes, with much finer sampling in the polar regions. Most MLS data products, including CIO, are reported on a fixed vertical pressure grid with six levels per decade change in pressure in the troposphere and stratosphere.

The MLS “Level 2” data (retrieved geophysical parameters and diagnostics at the measurement locations along the suborbital track) are generated from input “Level 1” data (calibrated radiances and engineering information) by the MLS data processing software. The MLS retrieval algorithms, described in detail by *Livesey et al.* [2006], are based on the standard optimal estimation method; they employ a two-dimensional approach that takes into account the fact that limb observations from consecutive scans cover significantly overlapping regions of the atmosphere. The data are divided into overlapping ‘chunks’ consisting of the measurements in a 15° span of great circle angle (typically about 10 vertical profiles); retrievals are performed for each of these chunks independently and then joined together to produce a complete set of output [*Livesey et al.*, 2006]. The results are reported in Level 2 Geophysical Product (L2GP) files, which are standard HDF-EOS version 5 files containing swaths in the Aura-wide standard format [*Livesey et al.*, 2007]. A separate L2GP file is produced for each standard MLS product for each day (00–24 h UT).

Reprocessing of the MLS data collected to date with the v2.2 algorithms is ongoing; however, at the time of writing (February 2007) only a small subset of the data, consisting of fewer than 100 days, has been reprocessed, with priority given to days for which correlative measurements exist. Although small compared to the entire MLS data record, this set of v2.2 days spans all seasons and is sufficient for thorough investigation of the MLS data quality.

2.2. MLS CIO Data Usage Guidelines

Along with the data fields, the L2GP files contain corresponding precision fields, which quantify the impact of radiance noise on the data and, particularly in regions with less measurement sensitivity, the contribution of a priori information. The data processing software flags the precision with a negative sign when the estimated precision is worse than 50% of the a priori precision; thus only data points for which the associated precision value is positive should be used.

Three additional data quality metrics are provided for every vertical profile of each product. ‘Status’ is a bit field indicating operational abnormalities or problems with the retrievals; see Table 1 for a complete description. Profiles for which ‘Status’ is an odd number should not be used in any scientific study. Nonzero but even values of ‘Status’ indicate that the profile has been marked as questionable, typically because the measurements may have been affected by the presence of thick clouds. Globally fewer than 1% of profiles are typically identified in this manner, and clouds generally have little influence on the stratospheric CIO data. Thus profiles with even values of ‘Status’ may be used without restriction.

The ‘Quality’ field describes the degree to which the measured MLS radiances have been fitted by the Level 2 algorithms. In theory, larger values of ‘Quality’ indicate generally good radiance fits, whereas values closer to zero indicate poorer radiance fits and thus less reliable data. In practice, low values of ‘Quality’ are not always associated with profiles that are obviously “bad”. As a precaution, we recommend rejecting profiles having ‘Quality’ values less than 0.8. This threshold for ‘Quality’ typically excludes $\sim 1\text{--}3\%$ of CIO profiles on a daily

basis; it is a conservative value that potentially discards a significant fraction of “good” data points while not necessarily identifying all “bad” ones.

Additional information on the success of the retrieval is conveyed by the ‘Convergence’ field, which compares the fit achieved for each ‘chunk’ of ~ 10 profiles to that expected by the retrieval algorithms; values around 1.0 typically indicate good convergence. We recommend rejecting profiles for which ‘Convergence’ exceeds 1.5. On a typical day this threshold for ‘Convergence’ discards 2–5% of the CIO profiles, some (but not all) of which are filtered out by the other quality control measures.

Finally, we note that the MLS data processing algorithms often produce negative mixing ratios, especially for noisy retrievals such as CIO when values are very low. Though unphysical, the negative mixing ratios must be retained in any scientific studies making use of averages of data, in order to avoid introducing positive biases into the MLS averages.

2.3. Signature of CIO in the MLS Radiances

Sample radiances from the 640-GHz region of the spectrum for a representative day during Antarctic winter are shown in Figure 1. More specifics about the MLS spectrometers, the spectral bands they cover, and their target molecules are given by *Waters et al.* [2006], and a full representation of the MLS spectral coverage superimposed on a calculated atmospheric spectrum is presented by *Read et al.* [2006]. The dominant spectral feature in the top panels is due to emission from an O_3 line near 650.7 GHz in the upper sideband (upper x-axis); the smaller peak at 649.45 GHz arises from a cluster of CIO lines. The left-hand plots show global average radiances, while the right-hand plots show the region poleward of $60^\circ S$ (where

chlorine has been converted from reservoir forms to ClO inside the Antarctic polar vortex) in order to emphasize the ClO spectral signature, which typically has an amplitude of $\sim 10\text{--}15$ K in the lower stratosphere when ClO is enhanced. The residuals shown in the lower panels indicate that on average the retrievals are fitting the radiances to within $\sim 5\%$ (~ 0.5 K) for these bands.

2.4. Precision, Spatial Resolution, and Vertical Range

The precision of the MLS ClO measurements is estimated empirically by computing the standard deviation of the descending (i.e., nighttime) profiles in the 20° -wide latitude band centered around the equator. For this region and time of day, natural atmospheric variability should be negligible relative to the measurement noise. As shown in Figure 2, the observed scatter in the v2.2 data is ~ 0.1 ppbv from 100 to 3 hPa, rising to ~ 0.3 ppbv at 1 hPa, above which it increases sharply. The scatter is essentially invariant with time, as seen by comparing the results for the different days shown in Figure 2.

The single-profile precision estimates cited here are, to first order, independent of latitude and season, but it should be borne in mind that the scientific utility of individual MLS profiles (i.e., signal to noise) varies with ClO abundance. Outside of the lower stratospheric winter polar vortices, within which ClO is often strongly enhanced, the single-profile precision exceeds typical ClO mixing ratios, necessitating the use of averages for scientific studies. In most cases, precision can be improved by averaging, with the precision of an average of N profiles being $1/\sqrt{N}$ times the precision of an individual profile (note that this is not the case for averages of successive along-track profiles, which are not completely independent because

of horizontal smearing).

The observational determination of the precision is compared in Figure 2 to the theoretical precision values reported by the Level 2 data processing algorithms. The predicted precision exceeds the observed scatter, particularly above 15 hPa, indicating that the a priori information and the vertical smoothing applied to stabilize the retrieval are influencing the results at these levels. Because the theoretical precisions take into account occasional variations in instrument performance, the best estimate of the precision of an individual data point is the value quoted for that point in the L2GP files, but it should be borne in mind that this approach slightly overestimates the actual measurement noise.

For comparison, Figure 2 also shows precision estimates for the v1.5 MLS CIO data. In terms of precision, the v2.2 CIO data are not greatly different from v1.5; other differences between the two versions are discussed in section 2.6.

As mentioned previously, the MLS retrieval algorithms employ a two-dimensional approach that accounts for the fact that the radiances for each limb scan are influenced by the state of the atmosphere at adjacent scans along the forward-looking instrument line of sight [Livesey *et al.*, 2006]. The resolution of the retrieved data can be described using ‘averaging kernels’ [e.g., Rodgers, 2000]; the two-dimensional nature of the MLS data processing system means that the kernels describe both vertical and horizontal resolution. Smoothing, imposed on the retrieval system in both the vertical and horizontal directions to enhance retrieval stability and precision, degrades the inherent resolution of the measurements. Consequently, the vertical resolution of the v2.2 CIO data, as determined from the full width at half maximum of the rows of the averaging kernel matrix shown in Figure 3, is $\sim 3\text{--}4.5$ km. Note that there

is considerable overlap in the averaging kernels for the 100 and 147 hPa retrieval surfaces, indicating that the 147 hPa retrieval does not provide completely independent information. Figure 3 also shows horizontal averaging kernels, from which the along-track horizontal resolution is determined to be ~ 250 – 500 km over most of the vertical range. The cross-track resolution, set by the width of the field of view of the 640-GHz radiometer, is ~ 3 km.

Although CIO is retrieved (and reported in the L2GP files) over the range from 147 to 0.001 hPa, based on the drop off in precision and resolution and the lack of independent information contributed by the measurements, the data are not deemed reliable at the extremes of the retrieval range. Thus we recommend that v2.2 CIO be used for scientific studies only at the levels between 100 and 1 hPa.

2.5. Quantification of Systematic Uncertainty

A major component of the validation of MLS data is the quantification of the various sources of systematic uncertainty. Systematic uncertainties arise from instrumental issues (e.g., radiometric calibration, field of view characterization), spectroscopic uncertainty, and approximations in the retrieval formulation and implementation. This section summarizes the relevant results of a comprehensive quantification of these uncertainties that was performed for all MLS products. More information on this assessment is given in Appendix A of Read et al. (*EOS Aura Microwave Limb Sounder Upper Tropospheric and Lower Stratospheric Humidity Validation*, submitted, 2007).

The impact on MLS measurements of radiance (or pointing where appropriate) of each identified source of systematic uncertainty has been quantified and modeled. These modeled

impacts correspond to either $2\text{-}\sigma$ estimates of uncertainties in the relevant parameters, or an estimate of their maximum reasonable errors based on instrument knowledge and/or design requirements. The effect of these perturbations on retrieved MLS products has been quantified for each source of uncertainty by one of two methods.

In the first method, sets of modeled errors corresponding to the possible magnitude of each uncertainty have been applied to simulated MLS cloud-free radiances, based on a model atmosphere, for a whole day of MLS observations. These sets of perturbed radiances have then been run through the routine MLS data processing algorithms, and the differences between these runs and the results of the ‘unperturbed’ run have been used to quantify the systematic uncertainty in each case. The impact of the perturbations varies from product to product and among uncertainty sources. Although the term ‘systematic uncertainty’ is often associated with consistent additive and/or multiplicative biases, many sources of ‘systematic’ uncertainty in the MLS measurement system give rise to additional scatter in the products. For example, although an error in the O_3 spectroscopy is a bias on the fundamental parameter, it has an effect on the retrievals of species with weaker signals (e.g., ClO) that is dependent on the amount and morphology of atmospheric ozone. The extent to which such terms can be expected to average down is estimated to first order by these ‘full up studies’ through their separate consideration of the bias and scatter each source of uncertainty introduces into the data. The difference between the retrieved product in the unperturbed run and the original ‘truth’ model atmosphere is taken as a measure of uncertainties due to retrieval formulation and numerics. To test the sensitivity of the retrieved mixing ratios to the a priori information, another retrieval of the unperturbed radiances is performed with the a priori adjusted by a

factor of 1.5.

In the second method, the potential impact of some remaining (typically small) systematic uncertainties has been quantified through calculations based on simplified models of the MLS measurement system [see Read et al., submitted, 2007]. Unlike the ‘full up studies’, these calculations only provide estimates of ‘gain uncertainty’ (i.e., possible multiplicative error) introduced by the source in question; this approach does not quantify possible biases or additional scatter for these minor sources of uncertainty.

Figure 4 summarizes the results of the error characterization for the MLS v2.2 ClO measurements. The colored lines show the magnitudes of expected biases, additional scatter, and possible scaling uncertainties the various errors may introduce into the data, and should be interpreted as 2- σ estimates of their probable magnitude. The dominant source of uncertainty throughout the profile originates from the spectral signature induced in the calibrated MLS radiances by departures from a linear response within the signal chains leading to gain compression (cyan lines). Other potentially significant sources of error include uncertainty in the field of view pointing offsets between the two 118-GHz radiometers and the 240-GHz radiometer (red lines), uncertainty in continuum emission/absorption and the width of the spectral line measured by MLS (green lines), and the impact of errors in O₃ (retrieved in the same phase as ClO [Livesey et al., 2006]) arising from errors in the O₃ lineshape (blue lines). Retrieval numerics and sensitivity of the MLS measurement system to a priori information (grey lines) contribute some scatter throughout the vertical range. Although these simulation results also suggest that retrieval numerics may lead to scaling errors of ± 35 –55% at 68 and 100 hPa, a reliable estimate is hampered by the (albeit geophysically appropriate) lack of

dynamic range in the ‘truth’ mixing ratios used for these levels, and the actual multiplicative error contributed by retrieval numerics is likely to be much smaller (e.g., $\sim \pm 20\%$ as at 46 hPa). Other potential sources of uncertainty, such as the presence of thick clouds associated with deep convection, are found to have a negligible impact.

In aggregate, systematic uncertainties are estimated to induce in the v2.2 ClO measurements biases of $\sim \pm 0.1$ ppbv from 100 to 32 hPa and less than ± 0.05 ppbv above 22 hPa and multiplicative errors of $\sim \pm 5\text{--}20\%$ throughout the stratosphere. The scatter introduced into the data by the various sources of uncertainty is estimated to be less than ± 0.04 ppbv throughout the vertical domain, a value substantially smaller than the empirical determination of the precision ($\sim 0.1\text{--}0.3$ ppbv) discussed in section 2.4.

As will be discussed in more detail in the following sections, a substantial ($\sim 0.1\text{--}0.4$ ppbv) negative bias is present in the v2.2 MLS ClO measurements at retrieval levels below 22 hPa. That such a significant feature in the data is not explained by the results presented in Figure 4 indicates limitations in our uncertainty quantification study. Potential but unaccounted for sources of error include contamination of the ClO retrieval from interfering species (other than ozone, the impact of which was quantified in Figure 4). Among these species, isotopic ozone is included in the MLS forward model, but, although it is known to be enhanced in the stratosphere [e.g., *Mauersberger et al.*, 2001], its values are constrained to natural terrestrial abundances, and the deviations from them have not been explored in the systematic error assessment. Other possible contaminant species are CH_3Cl and CH_3OH , which have clusters of lines in the image sideband but which are included in neither the v2.2 forward model nor this uncertainty analysis. In addition to interfering species, a potentially

significant but unquantified source of uncertainty is the accuracy with which the line shapes of strong ozone lines are modeled in the far wings, where the weak ClO lines are situated. Finally, it is also possible that the effects of some error sources, such as uncertainty in continuum emission/absorption and spectral line widths, while considered in the analysis in Figure 4, have been underestimated.

2.6. Comparison with v1.5 ClO Data

Early validation analyses of the v1.5 Aura MLS ClO data [Livesey *et al.*, 2005] revealed a persistent negative bias of as much as ~ 0.3 ppbv at low and middle latitudes in both daytime and nighttime mixing ratios at the lowest retrieval levels (below about 32 hPa). Comparisons with coincident measurements of ClO from the Submillimetre Radiometer (SMR) onboard the Odin satellite confirmed a systematic low bias of this magnitude in the MLS v1.5 data outside of the winter polar regions [Barret *et al.*, 2006].

Figure 5, which shows the comparison between v1.5 and v2.2 for 93 days for which both versions of data were available at the time of writing (February 2007), indicates that the negative bias has been exacerbated in v2.2, with the mixing ratios at 100 hPa more than 0.1 ppbv lower than they were in v1.5 in the global average. Differences between the v1.5 and v2.2 retrieval algorithms include changes in the representation of the continuum emission for the 640-GHz region, incorporation of additional O₃ lines, use of new direct laboratory measurements of O₃ line widths (including for isotopic and vibrational state lines) for several lines in this region, use of an updated version of the HITRAN database (2004 rather than 2000), and changes in the tangent pressure retrieval. Although these refinements

led to significant improvements in most MLS data products, cumulatively they resulted in an increase in the severity of the negative bias in ClO at the lowest retrieval levels.

Small differences between v1.5 and v2.2 are evident elsewhere in the profile as well; maximum mixing ratios at the profile peak in the lower stratosphere are slightly larger, whereas mixing ratios at the secondary peak near 2–3 hPa are slightly smaller (both by ~ 0.02 ppbv in the global mean) than they were in v1.5. The differences in peak values in both the upper and lower stratosphere can also be seen in the zonal mean fields in Figure 6.

Although v2.2 does not necessarily represent an advance over v1.5 in the case of ClO, other MLS data products have been improved substantially in v2.2. Use of a consistent dataset in scientific studies employing more than one MLS data product is highly desirable; moreover, production of the v1.5 dataset was discontinued after February 2007. We therefore recommend the use of v2.2, rather than v1.5, MLS ClO measurements for scientific studies.

2.7. Quantification of the Systematic Negative Bias

To quantify the magnitude of the negative bias in the v2.2 MLS ClO data and look for possible latitudinal and temporal variations in it, we have examined time series of data from the ascending (primarily daytime) and descending (primarily nighttime) sides of the orbit, as well as ascending-descending (day–night) difference values for all days that have so far been reprocessed in v2.2 (93 days spanning the time since launch in July 2004 through February 2007). The data have been binned and averaged in 10° -wide equivalent latitude bands between 80°S and 80°N on the 660, 580, 520, 460, and 410 K potential temperature surfaces, corresponding to pressure levels of 22, 32, 46, 68, and 100 hPa, respectively; as an

example, Figure 7 shows the results for 460 K. Averages were calculated in equivalent latitude (EqL, the latitude encircling the same area as a given contour of potential vorticity (PV) [Butchart and Remsberg, 1986]) rather than geographic latitude to obtain a vortex-centered view, ensuring that only similar air masses are averaged together and segregating the regions of ClO enhancement inside the winter polar vortex from the extra-vortex regions, where ClO mixing ratios are generally very low.

At the topmost level (not shown), nighttime mixing ratios are approximately zero at all EqLs and all seasons, except for a slight enhancement in the winter polar regions. At the levels below 660 K, however, a persistent negative bias is evident at low and middle latitudes, and at high latitudes outside winter. The magnitude of the bias in these regions is essentially the same in both daytime and nighttime mixing ratios, as expected since none of the potential sources of systematic uncertainty (see section 2.5) that could be giving rise to this bias are diurnally-varying. The bias increases in magnitude at the lower levels, reaching ~ 0.3 – 0.4 ppbv at 460 K (Figure 7) and ~ 0.4 – 0.5 ppbv at 410 K (not shown). With the exception of the polar regions during winter, the bias exhibits only small variations with either season or latitude, and is essentially eliminated by taking ascending–descending (day–night) differences.

At polar latitudes in both hemispheres, chlorine activation leads to substantial ClO enhancement during the winter. Figure 7 shows that the nighttime mixing ratios also exhibit nonnegligible positive values at this time, in some cases nearly as high as those observed during the day. It is well known from laboratory studies and in situ measurements that thermal decomposition of the ClO dimer, Cl_2O_2 , leads to increases in nighttime ClO abundances as temperatures increase over the range 190–215 K [e.g., Avallone and Toohey, 2001; World

Meteorological Organization, 2007, and references therein]. Similar increases in nighttime CIO mixing ratios in the winter polar vortices with increasing temperature have been seen in satellite observations from UARS MLS [e.g., *Waters et al.*, 1993] and Michelson Interferometer for Passive Atmospheric Sounding (MIPAS) [*Glatthor et al.*, 2004], and CIO mixing ratios of 0.7–0.8 ppbv have been measured at night inside the Arctic vortex by Odin/SMR [*Berthet et al.*, 2005], with maximum nighttime CIO abundances observed in the regions of highest temperature.

At the times/locations at which chlorine is not activated, the nighttime reservoir is ClONO_2 , and abundances of Cl_2O_2 are insignificant. In this case, the negative bias in the MLS CIO data can be eliminated by subtracting gridded or zonal-mean nighttime values from the individual daytime measurements. Figure 7, however, illustrates why taking day–night differences is not a practical approach inside the winter polar vortices: Subtraction of the nonnegligible nighttime CIO values substantially reduces the degree of chlorine activation indicated by the data. On the basis of a good correlation between MLS and SMR observations in the high latitude lower stratosphere, with both instruments measuring the same mean CIO enhancement in the Antarctic spring vortex, *Barret et al.* [2006] speculated that the negative bias was absent in v1.5 MLS CIO for conditions of strong chlorine activation. No instrumental or retrieval issues suggest, however, that the bias should disappear when CIO is enhanced. We therefore believe that it is necessary to subtract an estimate of the bias from the individual measurements at each of the affected levels, whether or not CIO is enhanced.

To determine the magnitude of the additive bias at each retrieval pressure level, we calculated daily averages of the CIO measurements in 20° -wide geographic latitude bins for

which the solar zenith angle (SZA) is greater than 100° and the local solar time is between
 22:00 and 04:00. To ensure that CIO was not enhanced, we restricted consideration to the
 days between 1 May and 1 November for the two northern high-latitude bins (50° – 70° N and
 70° – 90° N) and to the days between 1 November and 1 May for the two southern high-latitude
 bins (50° – 70° S and 70° – 90° S). For the other latitude bands the calculations were performed
 for all 93 days (spanning all seasons) for which v2.2 measurements were available at the time
 of writing. The average of the daily-mean values was then computed for each latitude band
 and pressure level. As shown in Figure 8, the bias in the CIO data worsens with increasing
 pressure. The dotted lines mark the magnitudes of the global-mean biases estimated by
 averaging together the values for the individual latitude bins at each level, which are -0.04,
 -0.14, -0.31, and -0.41 ppbv for the 32, 46, 68, and 100 hPa retrieval levels, respectively. No
 significant bias appears to be present in the data for the retrieval levels at or above 22 hPa.
 Figure 8 also shows, however, that the bias exhibits significant (up to 0.2 ppbv) latitudinal
 variation. In the lower stratosphere, CIO is mainly of interest in the winter polar regions, and
 using the global-mean bias estimates, which are strongly influenced by the larger values at
 low latitudes, may lead to overcompensation. Thus for most analyses it is more appropriate
 to estimate the magnitude of the bias by including only the middle and high latitude bins
 in the averages (i.e., excluding the 30° S– 30° N region), leading to values of -0.02, -0.12,
 -0.27, and -0.41 ppbv at 32, 46, 68, and 100 hPa, respectively (represented by the dashed
 lines in Figure 8). Further refinement in these bias estimates may be possible as more v2.2
 CIO data become available, including better understanding of the latitudinal and/or seasonal
 dependencies of their magnitudes.

The importance of accounting for the negative bias, especially in scientific studies examining CIO enhancement on potential temperature surfaces, is highlighted in Figure 9, which shows nighttime CIO measurements at 460 K as a function of temperature for representative days in the Arctic (top) and Antarctic (bottom) winters. In the panels on the left, in which the CIO data have not been corrected, the measurements appear to fall into two distinct populations, with the vortex (i.e., at high EqL in the winter hemisphere) data exhibiting little or no bias compared to data from outside the vortex. Interpretation of these plots is complicated by the fact that measurements from the 46-hPa retrieval surface, where the bias is smaller, are contributing to the values at 460 K inside the cold vortex, whereas measurements from the 68- and 100-hPa retrieval surfaces, where the bias is larger, are contributing to the values in the warmer extra-vortex regions. It is thus necessary to correct individual CIO measurements by subtracting the estimated negative bias at each of the affected retrieval levels before interpolation to potential temperature surfaces, as shown in the right-hand panels. The increase in nighttime high-EqL CIO with increasing temperature up to ~ 210 – 215 K is consistent with expectation as the equilibrium between CIO and its dimer shifts toward CIO and agrees well with the behavior seen in SMR measurements [Berthet *et al.*, 2005].

3. Comparison with UARS MLS Climatology

The MLS onboard UARS measured the global distribution of stratospheric CIO for much of the 1990s, albeit with approximately monthly gaps in high-latitude coverage arising from UARS yaw maneuvers and with significantly reduced temporal sampling in the latter half of the decade. A comprehensive overview of the seasonal, interannual, and interhemispheric

variations in ClO in EqL bands throughout the lower stratosphere (420–700 K potential temperature) was produced from the UARS MLS data by *Santee et al.* [2003]. Taking a similar approach with Aura MLS measurements provides a means of quantitatively comparing to the ClO climatology derived from UARS MLS data. The daily means in Figure 10 were computed by binning both the UARS and the Aura MLS ClO measurements into 5° EqL bands and averaging; results are shown for 10 EqL bands over annual cycles in both hemispheres. All UARS MLS data collected from 1991 through 2000 are represented by grey dots. To illustrate the degree of interannual variability in the Aura MLS data record, the v1.5 ClO measurements obtained in each year since launch in July 2004 are depicted in different shades of blue, with results from the v2.2 retrievals performed to date overlaid in red. Note that neither the v1.5 nor the v2.2 Aura MLS data have been corrected for the negative bias described in section 2.7. Data from both MLS instruments have been interpolated to the 520 K potential temperature surface (~46 hPa, 19 km) near the peak in the ClO vertical profile, using temperatures from the U.K. Met Office analyses [*Swinbank et al.*, 2002] for UARS MLS and from NASA’s Global Modeling and Assimilation Office Goddard Earth Observing System Version 4.0.3 (GEOS-4) [*Bloom et al.*, 2005] for Aura MLS.

Both the latitudinal variation of ClO and its evolution over an annual cycle match those in the climatology based on the multi-year UARS MLS dataset. Figure 10, however, clearly shows the pervasive low bias in both the v1.5 and the v2.2 Aura MLS ClO measurements in the lower stratosphere. Equivalent latitude means of ClO at other levels throughout the middle and upper stratosphere (not shown) indicate excellent agreement on average with the climatological values, but, as seen also in Figure 10, much less scatter is present in the v2.2

data than in the corresponding UARS MLS measurements.

4. Comparisons with Other Observations

In this section the accuracy of the Aura MLS v2.2 ClO measurements is assessed through comparisons with correlative datasets from a variety of different platforms, some of which were acquired in dedicated Aura validation campaigns. For most of these comparisons we use the traditional approach of considering matched pairs of profiles that are closely colocated both geographically and temporally. The coincidence criteria used to select the matches vary and are stated in each subsection below. In some cases, use of an additional filter based on the potential vorticity of the profiles (to ensure that only meteorologically consistent air masses are compared) was explored but was found to have little impact on the average differences.

4.1. Ground-Based Measurements

Measurements of ClO from a ground-based millimeter-wave spectrometer operating at Scott Base, Antarctica [e.g., *Solomon et al.*, 2000, 2002] are compared to Aura MLS data from nearby overpasses in a companion paper by Connor et al. (*Comparison of ClO measurements from the Aura MLS to ground-based microwave measurements at Scott Base, Antarctica in Spring 2005*, submitted, 2007). The intercomparisons cover the period of peak chlorine activation in September 2005, with measurements from 16 days passing all weather, quality control, and coincidence criteria during this interval. Day–night differences are taken for both instruments. Both v1.5 and a smaller subset of v2.2 MLS ClO data are examined; mean differences with the Scott Base values are nearly identical for the two MLS data versions. The

amplitude and the altitude of the secondary peak in the ClO profile in the upper stratosphere are in excellent agreement. In the lower stratosphere, large day-to-day variability in ClO during this period complicates interpretation of differences, but the mean agreement between the MLS and Scott Base values is nevertheless very good, with maximum mixing ratios from the ground-based instrument marginally larger than those from MLS. See Connor et al. [submitted, 2007] for further details on these comparisons.

4.2. Balloon Measurements

As part of the Aura validation effort, measurements of ClO were obtained near Aura overpasses from two remote sounding instruments during a balloon campaign carried out from Ft. Sumner, New Mexico, in September 2005. One of the instruments is the JPL MkIV solar occultation Fourier Transform Infrared (FTIR) spectrometer, which measures the 650–5650 cm^{-1} region with 0.01 cm^{-1} spectral resolution [Toon, 1991]. Profiles, obtained at sunrise or sunset, have a vertical resolution of 2–3 km. Systematic errors caused by spectroscopic uncertainties are as large as 15% for stratospheric ClO profiles. The other instrument is the JPL Submillimeterwave Limb Sounder-2 (SLS-2), a high-resolution heterodyne radiometer-spectrometer that measures limb thermal emission spectra of several species, including ClO, at frequencies near 650 GHz. A previous version of the instrument was described by Stachnik *et al.* [1999]; the newer SLS-2 incorporates an LHe-cooled superconductor insulator superconductor (SIS) quasi-optic mixer that has greater than 20 times the radiometric sensitivity of the earlier Schottky mixer instrument (system temperature T_{sys} of ~ 250 K double-sideband compared to ~ 5500 K). Vertical resolution of the SLS-2 data is

roughly 2–3 km below the balloon float altitude (~ 35 km) and 5–6 km above.

Comparisons between the balloon measurements and coincident MLS measurements are shown in Figure 11, where the MLS profiles are within 1° of latitude, 12° of longitude, and 8 hours of the balloon measurements. Good agreement is seen in the upper stratosphere, in terms of both the altitude and the approximate magnitude of the high-altitude peak. In the lower stratosphere, the significant negative bias in the MLS ClO retrievals below 32 hPa is evident. Correcting for this bias by subtracting its estimated value at each of the affected retrieval levels (section 2.7) leads to much better agreement, well within the combined error bars.

4.3. Aircraft Measurements

4.3.1. ASUR

Several aircraft campaigns have been conducted since the launch of Aura; although they have had strong science components, a significant focus of some of these campaigns has also been to collect observations to assist in the validation of Aura measurements. During one of these campaigns, the Polar Aura Validation Experiment (PAVE) in January/February 2005, the Airborne SUBmillimeter Radiometer (ASUR) made remote sensing measurements of ClO on flights of the NASA DC-8 research aircraft within and on the edge of the Arctic polar vortex [Kleinböhl *et al.*, 2005, see especially the auxiliary material]. Flights were coordinated to align along Aura instrument ground tracks near the time of the satellite overpass, as illustrated in Figure 12; note, however, that some of these flights were targeted toward validation of data from other Aura instruments, and in these cases the aircraft flight tracks are offset from those

of MLS. ASUR is a passive heterodyne instrument that measures ClO using the cluster of lines at 649.5 GHz; more information on the ASUR measurement and retrieval system is given by *Kleinböhl et al.* [2002]. Along with other stratospheric trace gases, vertical profiles of ClO are retrieved from spectrally-resolved pressure-broadened emission lines with a vertical resolution of 5–10 km calculated on a 2 km vertical grid over the range from ~ 15 to 50 km. The accuracy of the ClO measurements is estimated to be $\sim 10\%$ or 0.15 ppbv, whichever is higher.

Figures 13 and 14 compare the closest v2.2 MLS profiles to ASUR profiles obtained along Aura overpasses during PAVE (coincidence criteria: $\pm 2^\circ$ latitude, $\pm 4^\circ$ longitude, ± 2 hours); all comparisons are of profiles obtained in daylight. Figure 13 shows a few representative ClO profiles from three of the PAVE flights, selected to illustrate unenhanced, moderately enhanced, and strongly enhanced conditions. MLS, with considerably better vertical resolution, observes a much more sharply defined peak in ClO in the lower stratosphere than does ASUR. To account for the differing vertical resolutions of the two datasets, in Figure 13 we also show results from applying the ASUR averaging kernels to the MLS data; in general, degrading the resolution of the MLS ClO measurements in this manner significantly improves the comparisons. Agreement is typically very good near the secondary peak in the upper stratosphere, with average differences (Figure 14) between the MLS profiles multiplied by the ASUR averaging kernels and the ASUR profiles less than 0.1 ppbv (10%). The smoothed MLS profiles have smaller maximum abundances in the lower stratosphere, however, with average differences increasing below 30 km to greater than 0.4 ppbv (60%). The disparity between the two measurements in the lower stratosphere is significantly reduced but not eliminated when the negative bias in the v2.2 MLS ClO measurements is corrected.

4.3.2. HALOX

In situ measurements of highly enhanced ClO were made by the HALOX instrument onboard the stratospheric research aircraft M55 Geophysica during a flight inside the Arctic polar vortex on 7 March 2005 [von Hobe *et al.*, 2006, see also the auxiliary material], just prior to the major final warming. A detailed description of the HALOX instrument, which employs the chemical conversion resonance fluorescence technique to measure ClO, is provided by von Hobe *et al.* [2005]. ClO is measured with a time resolution of 10 s, a detection limit of 5 ppt, and an accuracy of $\sim 15\%$.

Using HALOX data for MLS validation purposes raises the issue of how to meaningfully compare the considerably coarser-resolution and less precise satellite measurements, which represent “average” conditions over a relatively large volume of air, with the highly precise in situ measurements, which represent conditions at a local point. Geophysical variability inevitably complicates interpretation of the comparison of datasets having sampling volumes of such vastly different scales. Furthermore, since the HALOX data were not obtained as part of a coordinated Aura validation program, coincident measurements are limited. In the analysis presented here, trajectory calculations have been used to map the air masses measured by HALOX to their locations at the time of the MLS overpasses; the closest coincidences between MLS and HALOX (advected to the MLS measurement times) occur on the ascend and dive segments of the flight (Figure 15a). Although both datasets represent daytime conditions, the HALOX data were obtained earlier in the morning at slightly higher SZAs (Figure 15b).

In Figure 15 we take a qualitative approach in which the in situ measurements are overlaid on the MLS ClO field geographically closest to the Geophysica flight track. Panel (c) shows the comparisons with the “raw” v2.2 MLS ClO data; in panel (d) the bias correction described in section 2.7 has been applied to the MLS data. Results are generally encouraging, especially at the lowest retrieval levels. HALOX frequently senses fine-scale structure not observable by MLS, but for the most part the spatial trends are roughly in agreement. MLS mixing ratios, however, are considerably lower than those recorded by HALOX at the highest altitudes (lowest pressures) attained by the Geophysica, even after the negative bias in the MLS data has been accounted for (Figure 15d).

A quantitative comparison for the separate flight segments is shown in Figure 16. As discussed by *Livesey et al.* [2007], proper comparison of MLS and in situ measurements involves a two-step process: the high-resolution in situ data are first downsampled to the MLS retrieval grid using a least squares fit, and the smoothed data are then multiplied by the MLS averaging kernels. After conversion to the coarse-resolution MLS grid, the HALOX measurements obtained during ascent (blue) match the coincident bias-corrected MLS profile to within 0.1 ppbv (15%) at 100 hPa, although lack of high-altitude HALOX measurements during this flight leg increases the uncertainty of the smoothed value at this level. The dive (red) provided close coincidences with two MLS profiles, which show excellent agreement (within $\sim 5\%$) at 100 hPa. At 68 hPa, however, HALOX sees ~ 0.25 ppbv ($\sim 15\text{--}20\%$) more ClO than indicated by MLS. This degree of agreement is within the combined accuracies of the two instruments.

4.4. Satellite Measurements

Satellite measurements provide the opportunity for more spatially and temporally extensive intercomparisons than those with ground-based, balloon, or aircraft datasets. They are also typically well matched to the MLS horizontal and vertical resolution. CIO is retrieved from spectra measured by MIPAS onboard the European Space Agency Environmental Satellite (Envisat), but, although these data have been presented for specific studies [*Glatthor et al.*, 2004; *von Clarmann et al.*, 2005], they are not readily available. The Atmospheric Chemistry Experiment Fourier Transform Spectrometer (ACE-FTS) on the Canadian Space Agency's SCISAT-1 mission also measures CIO, but these data remain a research product requiring special handling at this time [K. Walker, personal communication, 2005; *Dufour et al.*, 2006]. Therefore, we restrict our attention to comparisons with CIO measured by the SMR instrument onboard the Swedish-led Odin satellite [*Murtagh et al.*, 2002].

Odin was launched in February 2001 into a near-polar, sun-synchronous, ~600-km altitude orbit with an 18:00 ascending node. Odin operates in a time-sharing arrangement, alternating between astronomy and aeronomy modes; SMR observes limb thermal emission from CIO on roughly two measurement days per week using an auto-correlator spectrometer centered at 501.8 GHz. Operational Level 2 CIO retrievals are produced by the Chalmers University of Technology (Göteborg, Sweden). Retrievals from a similar data processing system in France were compared to MLS v1.5 CIO measurements by *Barret et al.* [2006]. The retrieval methodology and error characterization for the Chalmers version 1.2 data, and the differences between the French and Swedish data processing systems, are described in detail

by *Urban et al.* [2005]. The main differences between the Chalmers versions 1.2 and 2.0 are summarized by *Urban et al.* [2006]. Here we use Chalmers version 2.1 data, which for CIO are very similar to those in version 2.0, with differences typically smaller than ~ 50 pptv. The Chalmers version 2.0 CIO data have horizontal resolution of ~ 300 – 600 km, vertical resolution of 2.5 – 3 km, and single-scan precision better than 0.15 ppbv over the range from 15 to 50 km [*Urban et al.*, 2005, 2006]; similar values apply for the version 2.1 CIO data. The estimated total systematic error is less than 0.1 ppbv throughout the vertical range [*Urban et al.*, 2005, 2006]. Only good quality SMR data points are included in these comparisons (i.e., assigned flag `QUALITY = 0`, and a measurement response for each retrieved mixing ratio larger than 0.75 to ensure that the information has been derived from the measurements, with a negligible contribution from the climatological a priori profile [*Urban et al.*, 2005; *Barret et al.*, 2006]).

Figures 17 and 18 compare all coincident profiles obtained within $\pm 1^\circ$ in latitude, $\pm 4^\circ$ in longitude, and ± 12 hours from 49 days for which both SMR and v2.2 MLS data are available. All seasons are represented in this set of comparison days. Because the vertical resolution of the SMR CIO measurements is similar to that of the Aura MLS CIO measurements, for these comparisons the SMR profiles have been linearly interpolated in log-pressure to the fixed MLS retrieval pressure surfaces. The scatter plots of Figure 17 indicate good agreement in the general morphology of the CIO distribution, although the MLS data indicate stronger enhancements in the polar regions, particularly in the north; this apparent disparity is most likely related to solar zenith angle and local solar time differences between the matched profiles. The large negative bias in the MLS retrievals is evident in

the comparisons at the lowest levels, with average differences between MLS and SMR ClO exceeding 0.45 ppbv at 100 hPa (Figure 18). The discrepancy between the two measurements in the lower stratosphere is significantly reduced but not eliminated when the negative bias in the v2.2 MLS ClO measurements is corrected. A possible high bias of 0.1–0.2 ppbv in the SMR lower stratospheric measurements obtained outside the vortex during nighttime, when ClO abundances fall below the detection limit of the instrument [Berthet *et al.*, 2005], may largely explain the remaining offset. Differences are typically within ~ 0.05 ppbv at and above 32 hPa, with MLS values larger through most of this region; because of the very low mixing ratios, however, these values correspond to percent differences larger than 100% at some levels. As with the ground-based measurements, the amplitude and the altitude of the peak in the upper stratosphere are matched well.

The analysis presented in Figures 17 and 18 takes no account of the differences in solar zenith angle in the two ClO datasets. Barret *et al.* [2006] estimated that a 2° increase in SZA roughly corresponds to a 0.1 ppbv decrease in ClO, on the order of the estimated single-scan precision of the measurements; they concluded that a SZA coincidence criterion of $\pm 2^\circ$ is appropriate for an intercomparison of the ClO measurements from MLS and SMR. Because of differences in the observational patterns of the two instruments (both in sun-synchronous orbits), measurement points satisfying this SZA filter occur only at the highest latitudes, poleward of 70° in both hemispheres. In Figure 19 we summarize the comparison results obtained by imposing the additional SZA criterion and tightening the local solar time criterion to ± 2 hours. Such stringent coincidence criteria greatly reduce the number of matched points but significantly improve the agreement between the two datasets, with differences less than

0.05 ppbv (corresponding to $\sim 10\text{--}30\%$ over most of the profile) everywhere except at the bottom two levels, where the negative bias in the MLS data is largest. Correcting for the MLS bias enhances the agreement, although the results indicate that MLS actually overestimates ClO relative to SMR by more than 0.15 ppbv at 100 hPa.

5. Summary and Conclusions

We have assessed the quality and reliability of the Aura MLS version 2.2 (v2.2) ClO measurements. The standard ClO product is derived from radiances measured by the radiometer centered near 640 GHz; ClO is also retrieved using radiances from the 190-GHz radiometer, but these data have poorer precision. The MLS v2.2 ClO data are scientifically useful over the range 100 to 1 hPa. A summary of the precision and resolution (vertical and horizontal) of the v2.2 ClO measurements as a function of altitude is given in Table 2. The impact of various sources of systematic uncertainty has been quantified through a comprehensive set of retrieval simulations. Table 2 also includes estimates of the biases and scaling errors in the measurements compiled from this uncertainty analysis. The systematic uncertainty budget deduced through this set of simulations is, however, inconsistent with a significant artifact apparent in the measurements: a negative bias present in both daytime and nighttime mixing ratios below 22 hPa. In studies for which knowledge of lower stratospheric ClO mixing ratios to better than a few tenths of a ppbv is needed, it is recommended that this negative bias be corrected for by subtracting the value in Table 2 from the measurements at each affected level. The overall uncertainty for an individual data point is determined by taking the root sum square (RSS) of the precision, bias, and scaling error terms (for averages,

the single-profile precision value is divided by the square root of the number of profiles contributing to the average).

Comparisons with a climatology derived from the multi-year UARS MLS dataset and correlative datasets from a variety of different platforms have also been presented. A consistent picture emerges that both the amplitude and the altitude of the secondary peak in the CIO profile in the upper stratosphere are well determined by MLS. The latitudinal and seasonal variations in the CIO distribution in the lower stratosphere are also well determined, but the correlative comparisons confirm the existence of a substantial negative bias in the v2.2 MLS CIO data at the lowest retrieval levels.

Quality control should be implemented in any scientific studies using the MLS CIO measurements. Several metrics for evaluating data quality are provided along with the retrieved mixing ratios in the MLS Level 2 files. More detail on these quantities is given in section 2.2. Briefly, any data point for which any of the following conditions are met should be discarded:

1. the associated precision value is negative,
2. 'Status' is an odd number,
3. 'Quality' is less than 0.8, or
4. 'Convergence' is greater than 1.5.

Although in the case of CIO v2.2 does not necessarily represent an advance over the previous version, v1.5, other MLS data products have been improved substantially in v2.2.

Use of a consistent dataset in scientific studies employing more than one MLS data product is highly desirable; moreover, production of the v1.5 dataset was discontinued after February 2007. We therefore recommend the use of v2.2, rather than v1.5, MLS ClO measurements. Planned Version 3 algorithms may reduce the substantial negative bias present below 22 hPa and may also improve the ClO retrievals at 147 hPa.

Validation of satellite measurements is an ongoing process. It is important to continue to evaluate the quality of the MLS ClO dataset, especially in light of future refinements to the data processing software. The analyses presented here can be extended as more v2.2 data become available; at the time of writing (February 2007), fewer than 100 days of MLS data have been reprocessed to v2.2. Recent balloon flights from Kiruna, Sweden during the January/February 2007 campaign, continuing satellite missions, and planned deployments of various instruments during the upcoming International Polar Year, will all afford more opportunities for cross-comparisons.

Acknowledgments. We are very grateful to the MLS instrument and data operations and development team for their support through all the phases of the MLS project, in particular D. Flower, G. Lau, J. Holden, R. Lay, M. Loo, D. Miller, B. Mills, S. Neely, G. Melgar, A. Hanzel, M. Echeverri, E. Greene, A. Mousessian, and C. Vuu, and X. Sabouchi. We greatly appreciate the efforts of Bojan Bojkov and the Aura Validation Data Center (AVDC) team, whose work facilitated the MLS validation activities. Thanks to the Aura Project for their support throughout the years (before and after Aura launch), in particular M. Schoeberl, A. Douglass (also as co-chair of the Aura validation working group), E. Hilsenrath, and J. Joiner. We also acknowledge the support from NASA Headquarters: P. DeCola for MLS and Aura, and M. Kurylo, especially in relation to the Aura validation activities

656 and campaign planning efforts. The aircraft campaigns themselves involved tireless hours from various
657 coordinators, including E. Jensen and M. Schoeberl, as well as K. Thompson, and others involved with
658 campaign flight management and support. We express our thanks to the Columbia Scientific Balloon
659 Facility (CSBF) for providing operations services for the balloon experiments whose data are used
660 in this work. We are grateful to B. Connor for providing the Scott Base comparison results prior to
661 publication. Thanks to I. Mackenzie for helpful comments. Two anonymous reviewers are thanked
662 for their thoughtful comments. Odin is a Swedish-led satellite project funded jointly by the Swedish
663 National Space Board (SNSB), the Canadian Space Agency (CSA), the National Technology Agency
664 of Finland (Tekes) and the Centre National d'Études Spatiales (CNES) in France. Work at the Jet
665 Propulsion Laboratory, California Institute of Technology, was done under contract with the National
666 Aeronautics and Space Administration.

References

- Avallone, L. M., and D. W. Toohey, Tests of halogen photochemistry using in situ measurements of ClO and BrO in the lower polar stratosphere, *J. Geophys. Res.*, *106*, 10,411–10,421, 2001.
- Barret, B., et al., Intercomparisons of trace gas profiles from the Odin/SMR and Aura/MLS limb sounders, *J. Geophys. Res.*, *111*, D21302, doi:10.1029/2006JD007305, 2006.
- Berthet, G., et al., Nighttime chlorine monoxide observations by the Odin satellite and implications for the ClO/Cl₂O₂ equilibrium, *Geophys. Res. Lett.*, *32*, L11812, doi:10.1029/2005GL022649, 2005.
- Bloom, S. C., et al., The Goddard Earth Observing Data Assimilation System, GEOS DAS Version 4.0.3: Documentation and validation, *Tech. Rep. 104606 V26*, NASA, 2005.
- Butchart, N., and E. E. Remsberg, The area of the stratospheric polar vortex as a diagnostic for tracer transport on an isentropic surface, *J. Atmos. Sci.*, *43*, 1319–1339, 1986.
- Dufour, G., et al., Partitioning between the inorganic chlorine reservoirs HCl and ClONO₂ during the Arctic winter 2005 from the ACE-FTS, *Atmos. Chem. Phys.*, *6*, 2355–2366, 2006.
- Glatthor, N., et al., Spaceborne ClO observations by the Michelson Interferometer for Passive Atmospheric Sounding (MIPAS) before and during the Antarctic major warming in September/October 2002, *J. Geophys. Res.*, *109*, D11307, doi:10.1029/2003JD004440, 2004.
- Kleinböhl, A., et al., Vortexwide denitrification of the Arctic polar stratosphere in winter 1999/2000 determined by remote observations, *J. Geophys. Res.*, *107*, 8305, doi:10.1029/2001JD001042, 2002.
- Kleinböhl, A., et al., Denitrification in the Arctic mid-winter 2004/2005 observed by airborne submillimeter radiometry, *Geophys. Res. Lett.*, *32*, L19811, doi:10.1029/2005GL023408, 2005.

- 689 Livesey, N. J., W. V. Snyder, W. G. Read, and P. A. Wagner, Retrieval algorithms for the EOS
 690 Microwave Limb Sounder (MLS), *IEEE Trans. Geosci. Remote Sensing*, *44*, 1144–1155, 2006.
- 691 Livesey, N. J., et al., Version 1.5 Level 2 data quality and description document, *Tech. Rep. JPL*
 692 *D-32381*, Jet Propulsion Laboratory, 2005, available from <http://mls.jpl.nasa.gov>.
- 693 Livesey, N. J., et al., Version 2.2 Level 2 data quality and description document, *Tech. Rep. JPL*
 694 *D-32381*, Jet Propulsion Laboratory, 2007, available from <http://mls.jpl.nasa.gov>.
- 695 Mauersberger, K., P. Lämmerzahl, and D. Krankowsky, Stratospheric ozone isotope enrichments —
 696 revisited, *Geophys. Res. Lett.*, *28*, 3155–3158, 2001.
- 697 Murtagh, D., et al., An overview of the Odin atmospheric mission, *Can. J. Phys.*, *80*, 309–319, 2002.
- 698 Read, W. G., Z. Shippony, M. J. Schwartz, N. J. Livesey, and W. V. Snyder, The clear-sky unpolarized
 699 forward model for the EOS Aura Microwave Limb Sounder (MLS), *IEEE Trans. Geosci.*
 700 *Remote Sensing*, *44*, 1367–1379, 2006.
- 701 Rodgers, C. D., *Inverse Methods for Atmospheric Sounding: Theory and Practice*, World Sci.,
 702 Singapore, 2000.
- 703 Santee, M. L., G. L. Manney, J. W. Waters, and N. J. Livesey, Variations and climatology of ClO in
 704 the polar lower stratosphere from UARS Microwave Limb Sounder measurements, *J. Geophys.*
 705 *Res.*, *108*, 4454, doi:10.1029/2002JD003335, 2003.
- 706 Santee, M. L., et al., Polar processing and development of the 2004 Antarctic ozone hole: First results
 707 from MLS on Aura, *Geophys. Res. Lett.*, *32*, L12817, doi:10.1029/2005GL022582, 2005.
- 708 Schoeberl, M. R., et al., Chemical observations of a polar vortex intrusion, *J. Geophys. Res.*, *111*,
 709 D20306, doi:10.1029/2006JD007134, 2006a.

- 710 Schoeberl, M. R., et al., Overview of the EOS Aura mission, *IEEE Trans. Geosci. Remote Sensing*, 44,
711 1066–1074, 2006b.
- 712 Solomon, P., J. Barrett, B. Conner, S. Zoonematkermani, A. Parrish, A. Lee, J. Pyle, and
713 M. Chipperfield, Seasonal observations of chlorine monoxide in the stratosphere over
714 Antarctica during the 1996–1998 ozone holes and comparison with the SLIMCAT three-
715 dimensional model, *J. Geophys. Res.*, 105, 28,979–29,001, 2000.
- 716 Solomon, P., B. Connor, J. Barrett, T. Mooney, A. Lee, and A. Parrish, Measurements of stratospheric
717 ClO over Antarctica in 1996–2000 and implications for ClO dimer chemistry, *Geophys. Res.*
718 *Lett.*, 29, 10.1029/2002GL015232, 2002.
- 719 Solomon, S., Stratospheric ozone depletion: A review of concepts and history, *Rev. Geophys.*, 37,
720 275–316, 1999.
- 721 Stachnik, R. A., R. Salawitch, A. Engel, and U. Schmidt, Measurements of chlorine partitioning in the
722 winter Arctic stratosphere, *Geophys. Res. Lett.*, 26, 3093–3096, 1999.
- 723 Swinbank, R., N. B. Ingleby, P. M. Boorman, and R. J. Renshaw, A 3D variational data assimilation
724 system for the stratosphere and troposphere, *Tech. Rep. 71*, Met Office Numerical Weather
725 Prediction Forecasting Research Scientific Paper, 2002.
- 726 Toon, G. C., The JPL MkIV interferometer, *Opt. Photon. News*, 2, 19–21, 1991.
- 727 Urban, J., et al., Odin/SMR limb observations of stratospheric trace gases: Level 2 processing of ClO,
728 N₂O, HNO₃, and O₃, *J. Geophys. Res.*, 110, D14307, doi:10.1029/2004JD005741, 2005.
- 729 Urban, J., et al., Odin/SMR limb observations of trace gases in the polar lower stratosphere
730 during 2004–2005, in *Proc. ESA First Atmospheric Science Conference*, 8–12 May 2006,

- 731 *Frascati, Italy*, edited by H. Lacoste, European Space Agency publications, ESA-SP-628,
732 ISBN-92-9092-939-1, ISSN-1609-042X, 2006.
- 733 von Clarmann, T., et al., Experimental evidence of perturbed odd hydrogen and chlorine
734 chemistry after the October 2003 solar proton events, *J. Geophys. Res.*, *110*, A09S45,
735 doi:10.1029/2005JA011053, 2005.
- 736 von Hobe, M., J.-U. Grooß, R. Müller, S. Hrechanyy, U. Winkler, and F. Stroh, A re-evaluation of
737 the ClO/Cl₂O₂ equilibrium constant based on stratospheric in-situ observations, *Atmos. Chem.*
738 *Phys.*, *5*, 693–702, 2005.
- 739 von Hobe, M., et al., Severe ozone depletion in the cold Arctic winter 2004–05, *Geophys. Res. Lett.*,
740 *33*, L17815, doi:10.1029/2006GL026945, 2006.
- 741 Waters, J. W., Microwave limb sounding, in *Atmospheric Remote Sensing by Microwave Radiometry*,
742 edited by M. A. Janssen, chap. 8, pp. 383–496, John Wiley, New York, 1993.
- 743 Waters, J. W., L. Froidevaux, W. G. Read, G. L. Manney, L. S. Elson, D. A. Flower, R. F. Jarnot, and
744 R. S. Harwood, Stratospheric ClO and ozone from the Microwave Limb Sounder on the Upper
745 Atmosphere Research Satellite, *Nature*, *362*, 597–602, 1993.
- 746 Waters, J. W., et al., The Earth Observing System Microwave Limb Sounder (EOS MLS) on the Aura
747 satellite, *IEEE Trans. Geosci. Remote Sensing*, *44*, 1075–1092, 2006.
- 748 World Meteorological Organization, *Scientific assessment of ozone depletion: 2006*, Global Ozone
749 Res. and Monit. Proj. Rep. No. 50, Geneva, 2007.
-
- 750 M. L. Santee (corresponding author), R. E. Cofield, D. T. Cuddy, W. H. Daffer, B. J. Drouin,
751 L. Froidevaux, R. A. Fuller, R. F. Jarnot, A. Kleinböhl, B. W. Knosp, A. Lambert, N. J. Livesey,

V. S. Perun, W. G. Read, W. V. Snyder, R. A. Stachnik, P. C. Stek, R. P. Thurstans, G. C. Toon,
 P. A. Wagner, and J. W. Waters, Jet Propulsion Laboratory, 4800 Oak Grove Drive, Pasadena,
 CA 91109, USA. (mls@mls.jpl.nasa.gov)

B. Barret and P. Ricaud, Laboratoire d'Aérodynamique, CNRS, 14 avenue Edouard Belin,
 Toulouse, F-31400 France.

H. Küllmann, Institute of Environmental Physics, University of Bremen, Bremen, Germany.

J. Kuttippurath, LMD/CNRS Ecole Polytechnique, Palaiseau, France.

G. L. Manney, Department of Physics, New Mexico Institute of Mining and Technology,
 Socorro, NM 87801, USA.

D. Murtagh and J. Urban, Department of Radio and Space Science, Chalmers University of
 Technology, SE-41296 Göteborg, Sweden.

M. von Hobe, Institut für Chemie und Dynamik der Geosphäre I: Stratosphäre (ICG-I),
 Forschungszentrum Jülich, D-52425 Jülich, Germany.

Received _____

This manuscript was prepared with AGU's L^AT_EX macros v5, with the extension package
 'AGU⁺⁺' by P. W. Daly, version 1.6b from 1999/08/19.

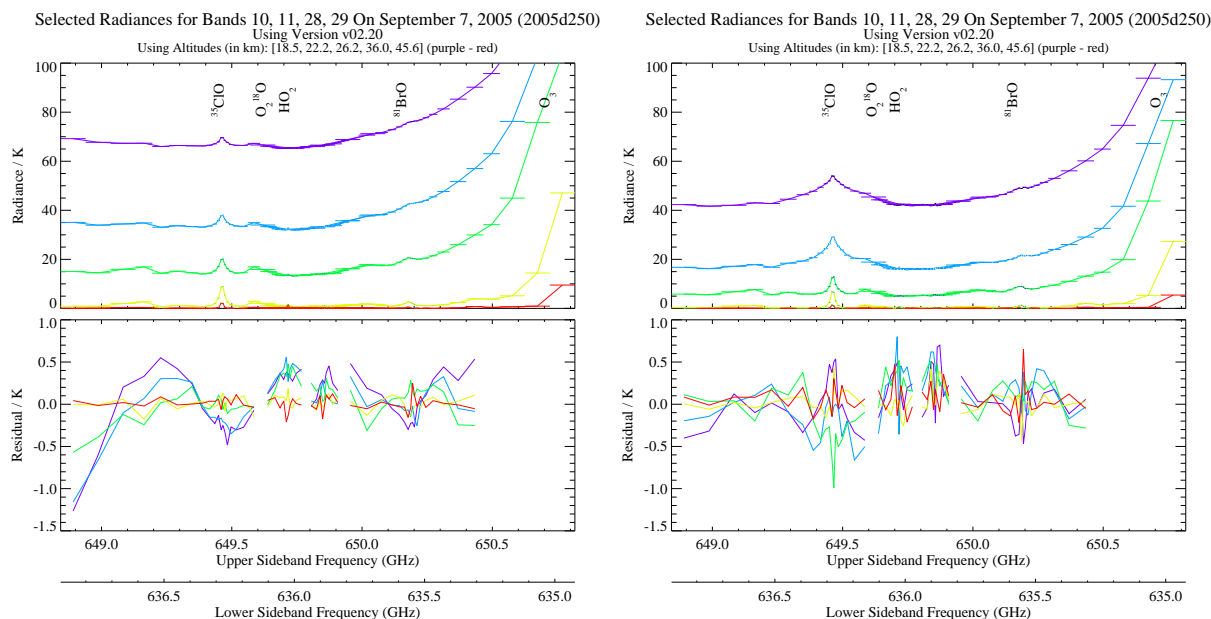
768 **Figure Captions**

Figure 1. Sample radiances and residuals from the Aura MLS 640-GHz radiometer for Bands 10 and 11 for ascending (daytime) data averaged over (left) the entire globe and (right) latitudes poleward of 60°S. (Top panels) Average radiances for a representative day with substantial ClO enhancement in the Antarctic polar vortex (7 September 2005), expressed as brightness temperature (in K), for five selected tangent point altitudes from 18.5 km (purple) to 45.6 km (red). The MLS signal is a combination of incoming radiance at frequencies above (upper sideband, upper x-axis) and below (lower sideband, lower x-axis) the 642.870 GHz local oscillator. The widths of the various MLS spectral channels are denoted by the horizontal bars. (Bottom panels) The average residual of the fit achieved by the MLS version 2.2 (v2.2) retrieval algorithms. Residuals for channels not used in the retrievals are not shown.

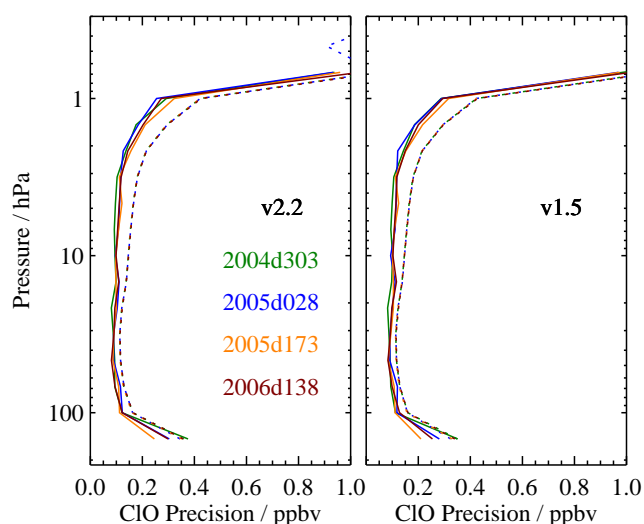


Figure 2. Precision of the (left) v2.2 and (right) v1.5 MLS ClO measurements for four representative days (see legend). Solid lines depict the observed scatter in nighttime-only measurements obtained in a narrow equatorial band (see text); dotted lines depict the theoretical precision estimated by the retrieval algorithm.

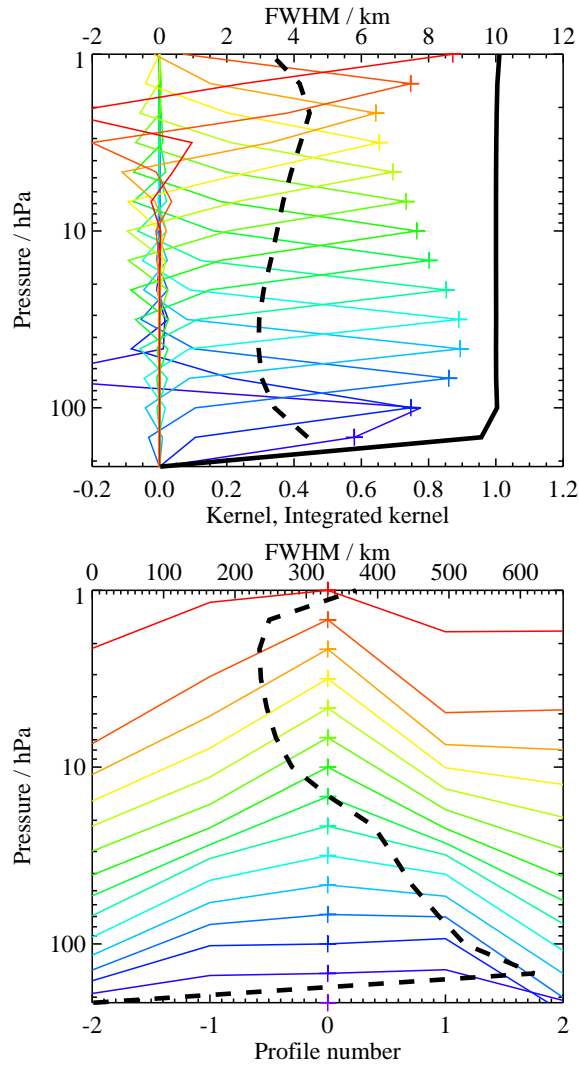


Figure 3. Typical two-dimensional (vertical and horizontal along-track) averaging kernels for the MLS v2.2 ClO data at 70°N; variation in the averaging kernels is sufficiently small that these are representative for all profiles. Colored lines show the averaging kernels as a function of MLS retrieval level, indicating the region of the atmosphere from which information is contributing to the measurements on the individual retrieval surfaces, which are denoted by plus signs in corresponding colors. The dashed black line indicates the resolution, determined from the full width at half maximum (FWHM) of the averaging kernels, approximately scaled into kilometers (top axis). (Top) Vertical averaging kernels (integrated in the horizontal dimension for five along-track profiles) and resolution. The solid black line shows the integrated area under each kernel (horizontally and vertically); values near unity imply that the majority of information for that MLS data point has come from the measurements, whereas lower values imply substantial contributions from a priori information. (Bottom) Horizontal averaging kernels (integrated in the vertical dimension) and resolution. The individual horizontal averaging kernels are scaled in the vertical direction such that a unit change is equivalent to one decade in pressure.

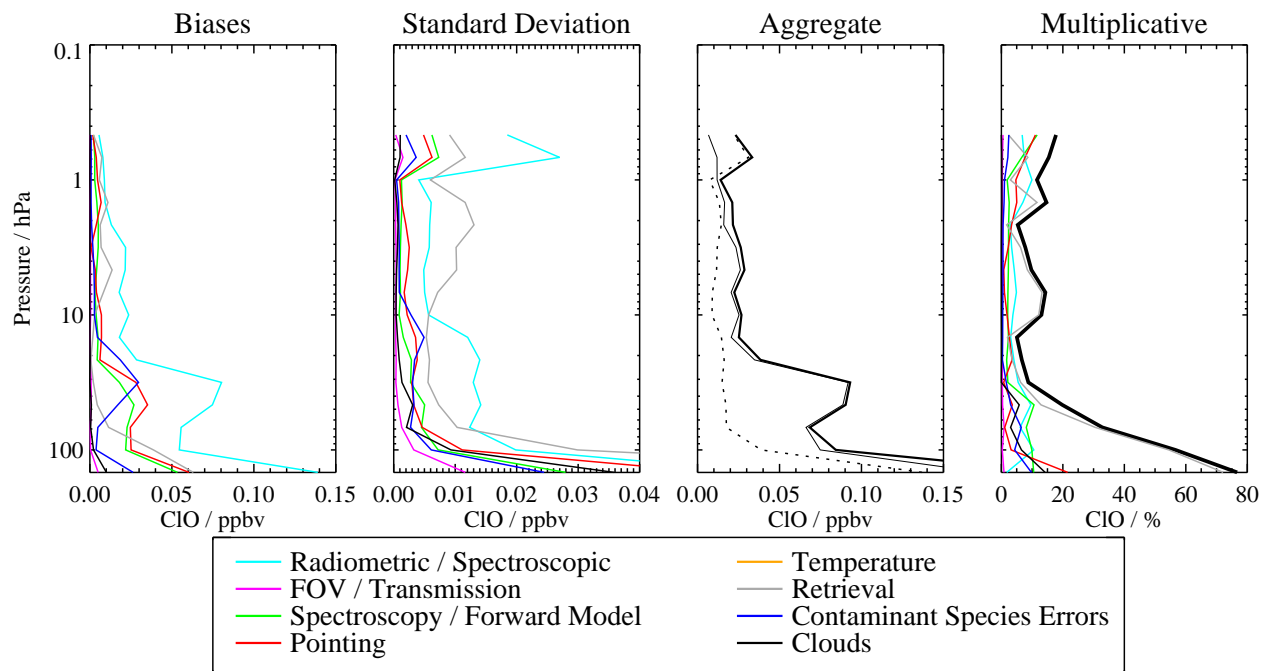


Figure 4. The estimated impact ($2\text{-}\sigma$) of various families of systematic uncertainty on the MLS ClO observations. The first two panels show the (first) possible biases and (second) standard deviation of the additional scatter introduced by the various families of uncertainty, with each family denoted by a different colored line. Cyan lines denote uncertainties in MLS radiometric and spectral calibration. Magenta lines show uncertainties associated with the MLS field of view and antenna transmission efficiency. Red lines depict errors associated with MLS pointing uncertainty. The impacts of uncertainties in spectroscopic databases and forward model approximations are denoted by the green line, while those associated with retrieval formulation are shown in grey. The gold lines indicate uncertainty resulting from errors in the MLS temperature product, while the blue lines show the impact of similar ‘knock on’ errors in other species. Finally, the typical impact of cloud contamination is denoted by the black line. (Third) The root sum square (RSS) of all the possible biases (thin solid line), all the additional scatter (thin dotted line), and the RSS sum of the two (thick solid line). (Fourth) The scaling uncertainty introduced by the various families of errors, with the thick black line showing the RSS of all the reported scaling uncertainties.

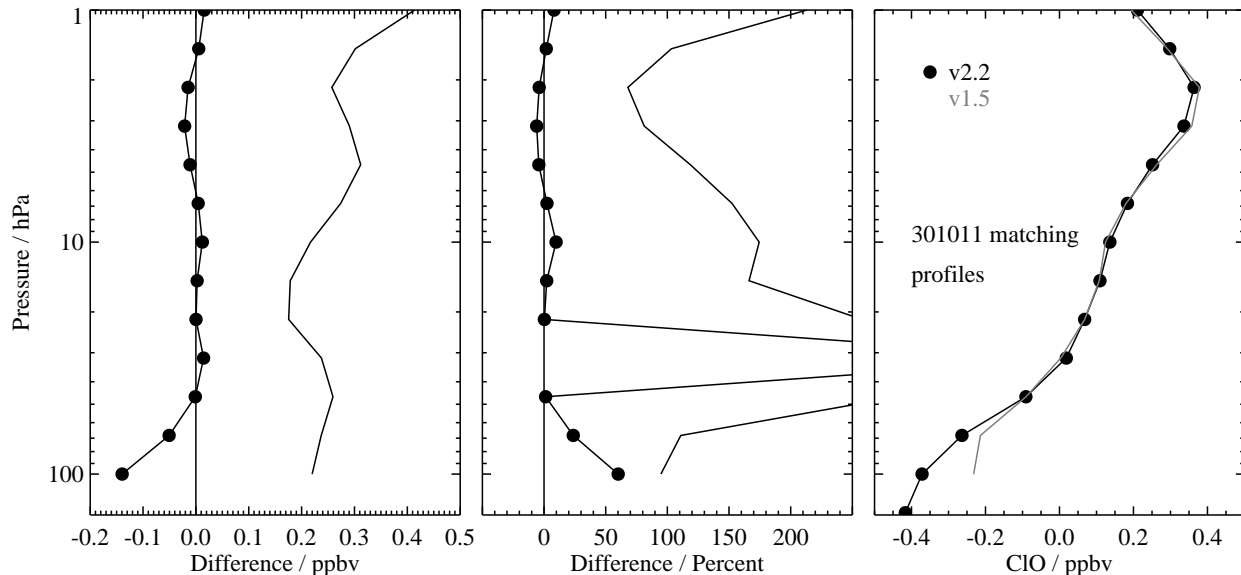


Figure 5. Comparison of v2.2 and v1.5 Aura MLS ClO measurements from 93 days for which both versions of data were available at the time of writing (February 2007). (Left) Absolute differences (v2.2–v1.5); the black line with dots (symbols indicate MLS retrieval surfaces) shows mean differences and the solid black line shows the standard deviation of the differences. (Middle) Same, for percent differences (computed relative to v1.5). Large percent differences at the 32 hPa retrieval level arise because ClO mixing ratios are very low in this region. (Right) Global mean profiles for v2.2 (black, with dots) and v1.5 (grey). Note that the ClO retrieval has been extended down to 147 hPa in v2.2.

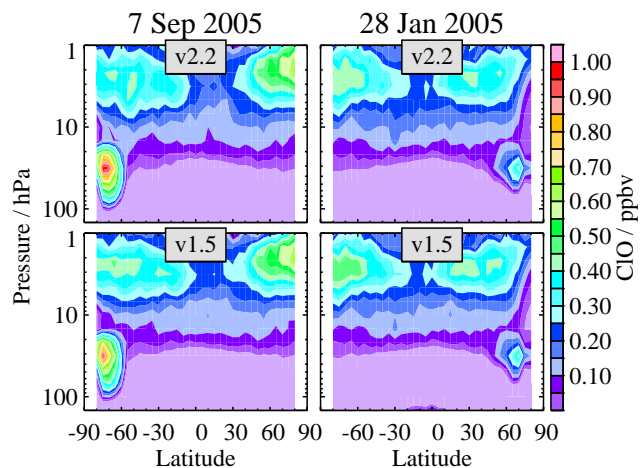


Figure 6. Zonal-mean cross sections of (top) v2.2 and (bottom) v1.5 Aura MLS daytime (ascending) ClO for two selected days, chosen to illustrate ClO enhancement in the (left) southern (7 September 2005) and (right) northern (28 January 2005) winter polar regions.

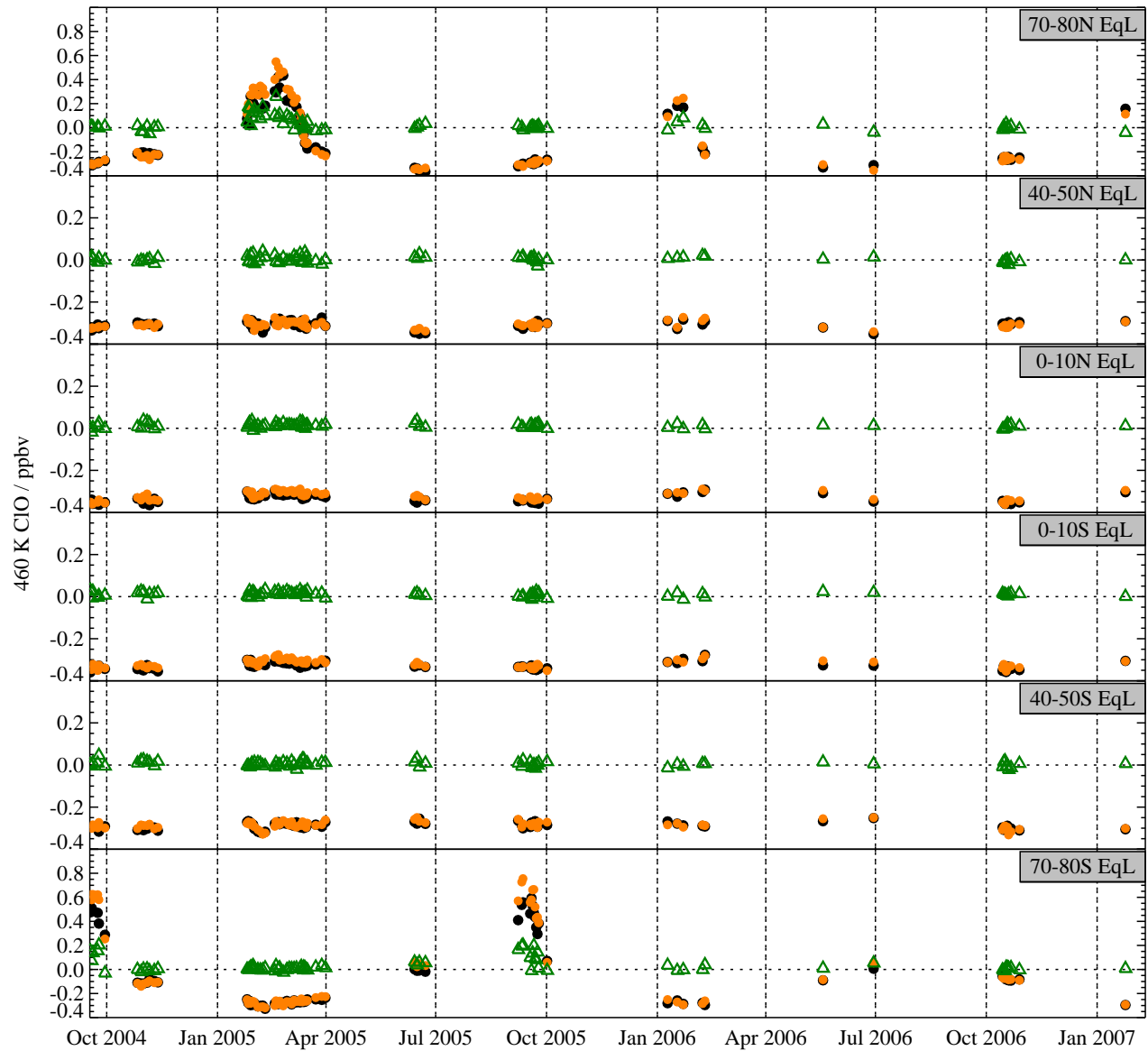


Figure 7. Time series of MLS v2.2 ClO measurements at 460 K potential temperature (corresponding to ~ 68 hPa, 17 km) for the 93 days processed at the time of writing. Temperatures from NASA's Global Modeling and Assimilation Office Goddard Earth Observing System Version 4.0.3 (GEOS-4) were used to interpolate the data to potential temperature. Daily means were calculated by binning the measurements into 10° -wide equivalent latitude (EqL) bands and averaging; high, middle, and low EqL bands are shown for each hemisphere. Orange dots depict averages of data from the ascending (primarily daytime) side of the orbit, whereas black dots depict averages of data from the descending (primarily nighttime) side of the orbit. Differences of the daily ascending and descending averages (day–night) are shown with open green triangles. Note that the y-axis ranges for the two high-latitude bins differ from those of the other bands.

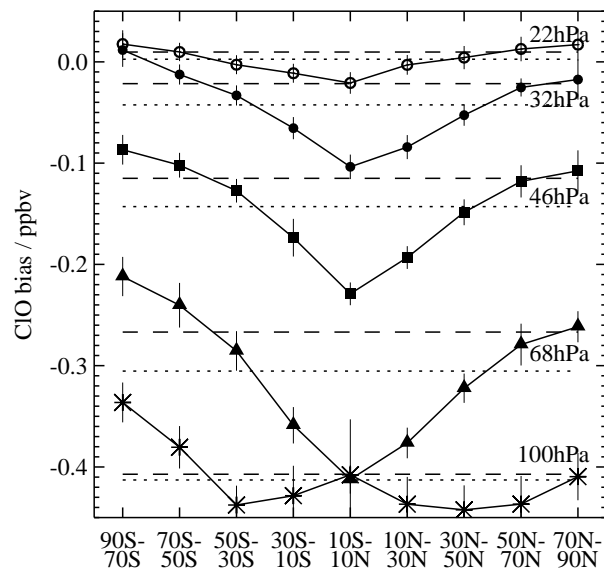


Figure 8. Estimates of the bias in MLS v2.2 CIO data in 20°-wide geographic latitude bands at 100, 68, 46, 32, and 22 hPa (labelled lines drawn with different symbols). Vertical error bars reflect the standard deviations in the averages of the daily-mean values. The magnitudes of the global-mean bias at each pressure level are denoted by the dotted lines; the dashed lines represent the average biases calculated using only the middle and high latitude bins (i.e., excluding the 30°S–30°N region).

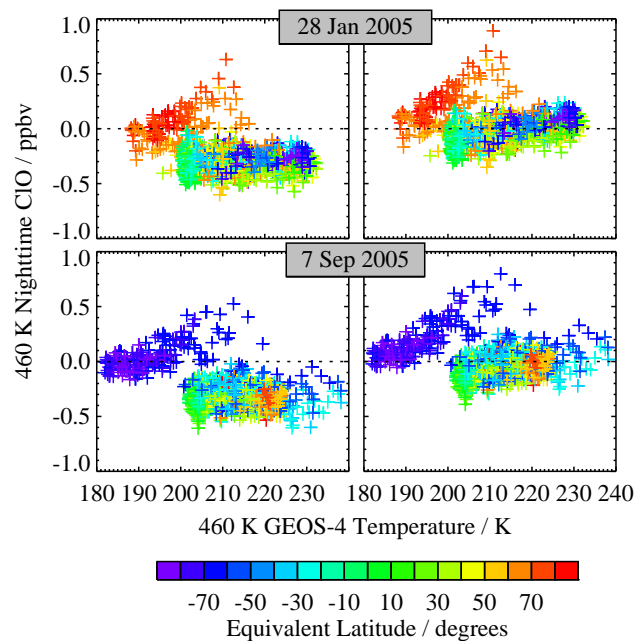


Figure 9. MLS v2.2 nighttime (solar zenith angle (SZA) > 100°, local solar time (LST) between 22:00 and 04:00) CIO measurements at 460 K as a function of GEOS-4 temperature for two representative days during (top) northern (28 January 2005) and (bottom) southern (7 September 2005) winter. Data points are color-coded by equivalent latitude. The panels on the left show uncorrected MLS data; the panels on the right show corrected data, for which the estimate of the bias (based on the middle and high latitude values; dashed lines in Figure 8) has been subtracted from the individual “raw” mixing ratios at each affected retrieval pressure level prior to interpolation to potential temperature.

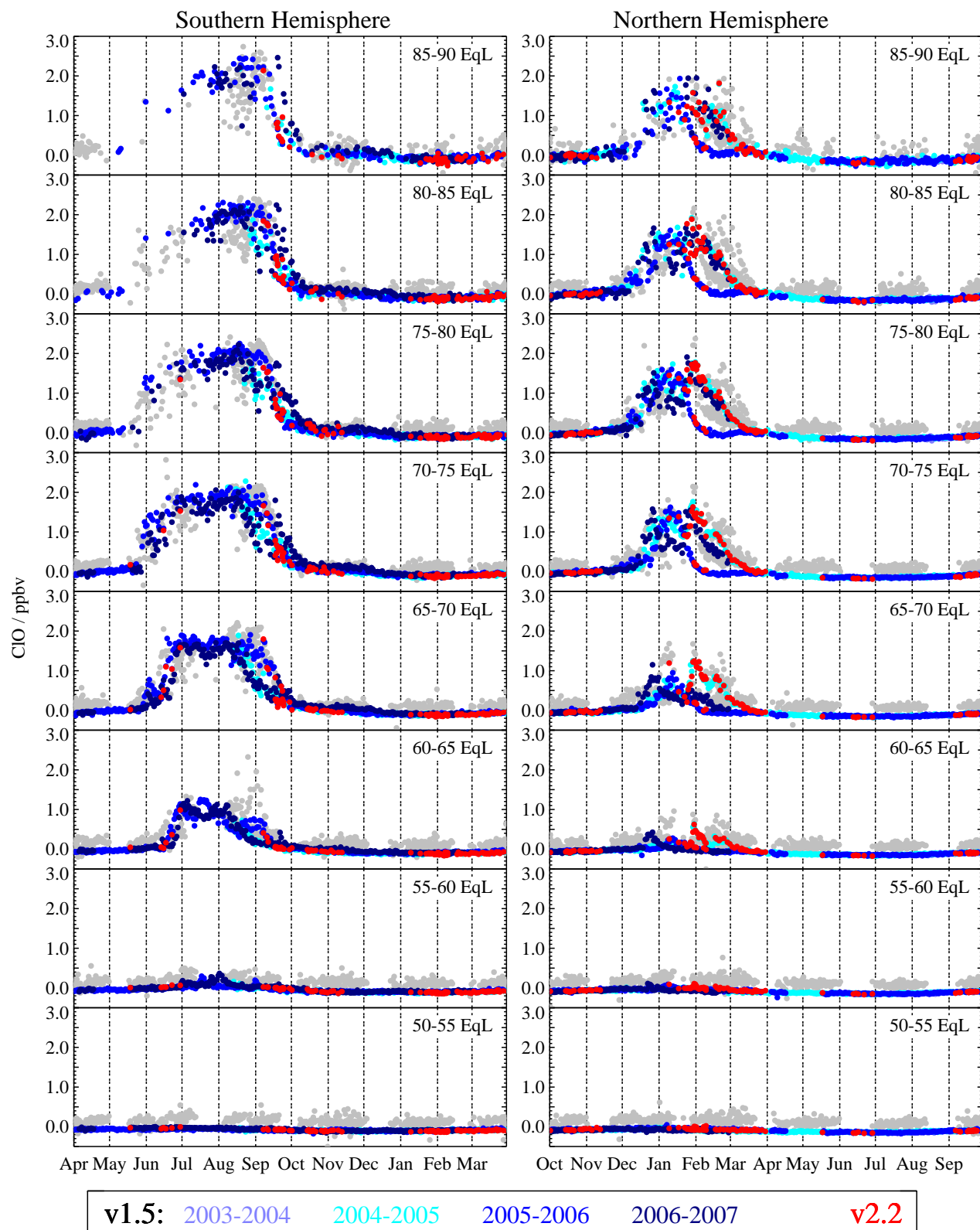


Figure 10. Time series of MLS CIO measurements at 520 K potential temperature (corresponding to ~ 46 hPa, 19 km) for the (left) Southern and (right) Northern Hemispheres. Daily means were calculated by binning the measurements into 5° -wide EqL bands and averaging. Grey dots depict version 5 UARS MLS CIO data taken over the period 1991–2000; blue dots depict v1.5 Aura MLS CIO data, with different shades of blue representing different years as indicated in the legend, and red dots depict v2.2 Aura MLS data for the 93 days processed at the time of writing. Only daytime data were included in the averages ($\text{SZA} < 92^\circ$, $10:00 < \text{LST} < 15:00$). Dashed vertical lines demark calendar months.

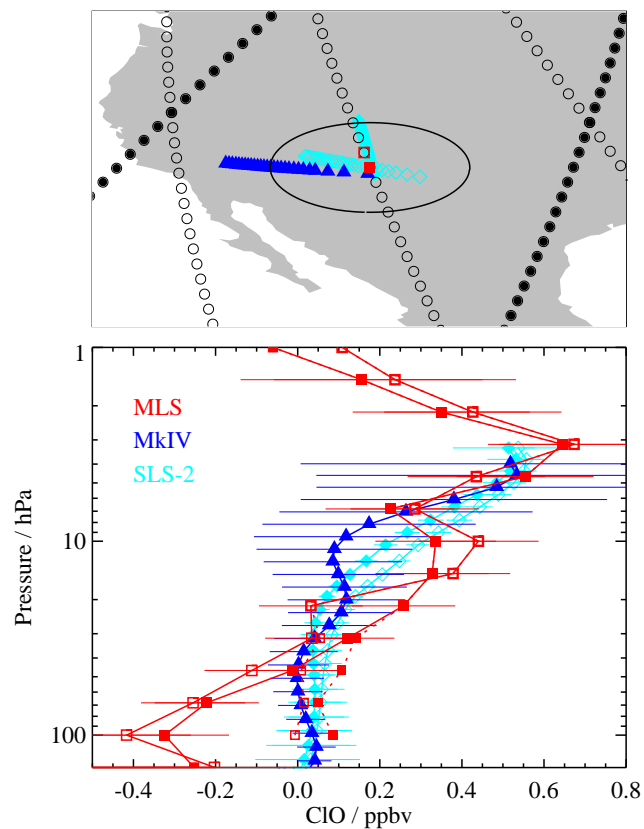


Figure 11. (Top) Path traversed by measurements from the balloon-borne MkIV (blue triangles) and SLS-2 (cyan diamonds) instruments during the flight from Ft. Sumner, NM, on 20–21 September 2005. Measurement tracks from nearby MLS ascending (daytime, open circles) and descending (nighttime, filled circles) orbit legs are also shown. The two MLS data points closest to the balloon measurements geographically and temporally are indicated by red squares, with the closer one denoted by a filled symbol; the 500-km radius around the closest MLS point is overlaid in black. (Bottom) Profiles of CIO, corresponding to the symbols in the top panel, from MLS (red squares; solid lines with larger symbols show “raw” MLS data, dotted lines with smaller symbols show MLS data corrected for the negative bias as described in section 2.7), MkIV (blue triangles), and SLS-2 (cyan open and filled diamonds). Error bars represent the estimated precisions of each instrument, taken from the data files (for clarity, they have been omitted from the corrected MLS profiles).

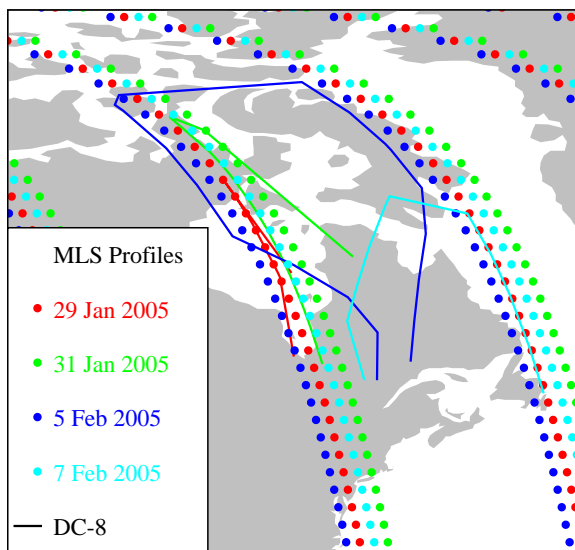


Figure 12. Flight tracks (lines color-coded by date) of the NASA DC-8 aircraft during the Polar Aura Validation Experiment (PAVE) mission conducted from Portsmouth, New Hampshire in January/February 2005. Only flights on days for which both MLS v2.2 and ASUR data are available are shown. The MLS ground tracks on these days are indicated by solid dots in corresponding colors.

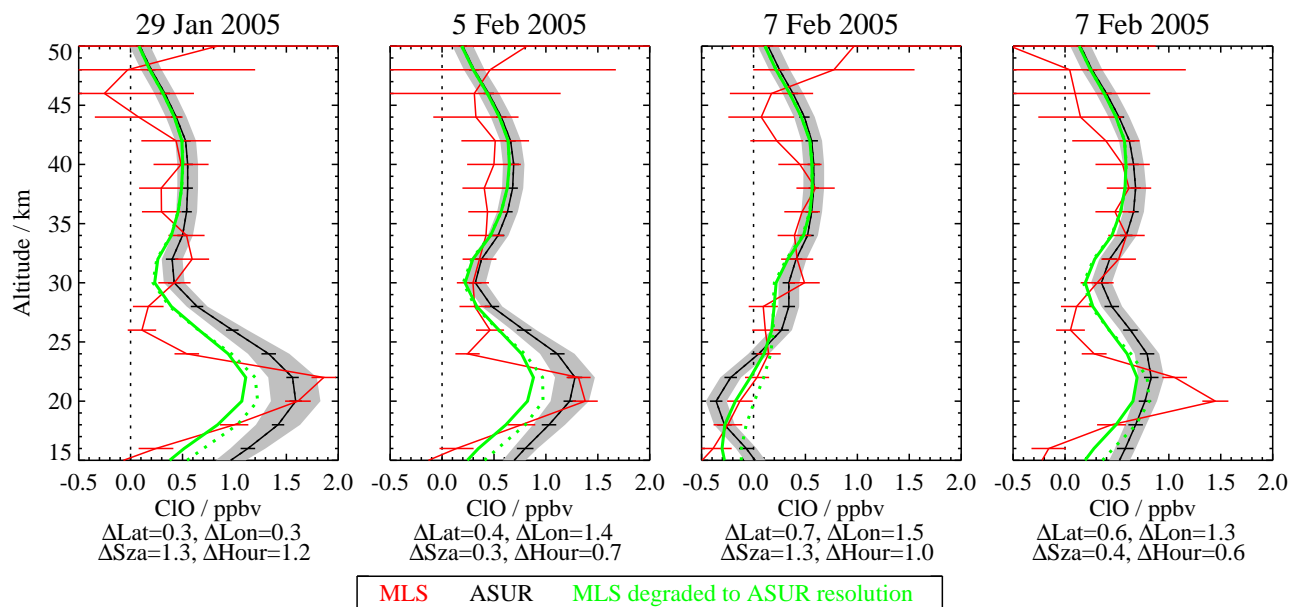


Figure 13. Comparison of the closest MLS v2.2 CIO profiles to the ASUR measurements taken along Aura overpasses during the PAVE campaign in January/February 2005; individual panels show four representative comparisons from three flights. ASUR profiles are shown in black, with grey shading indicating the accuracy and error bars indicating the 1- σ statistical error, derived from the measurement noise. MLS profiles are shown in red, with error bars representing the estimated precision of the CIO data reported by the retrieval system. MLS profiles multiplied by the ASUR averaging kernels are shown in green; solid lines show “raw” MLS CIO values, dotted lines show MLS data corrected for the negative bias as described in section 2.7. The separation between the MLS and ASUR profiles in latitude, longitude, time, and solar zenith angle is noted for each case.

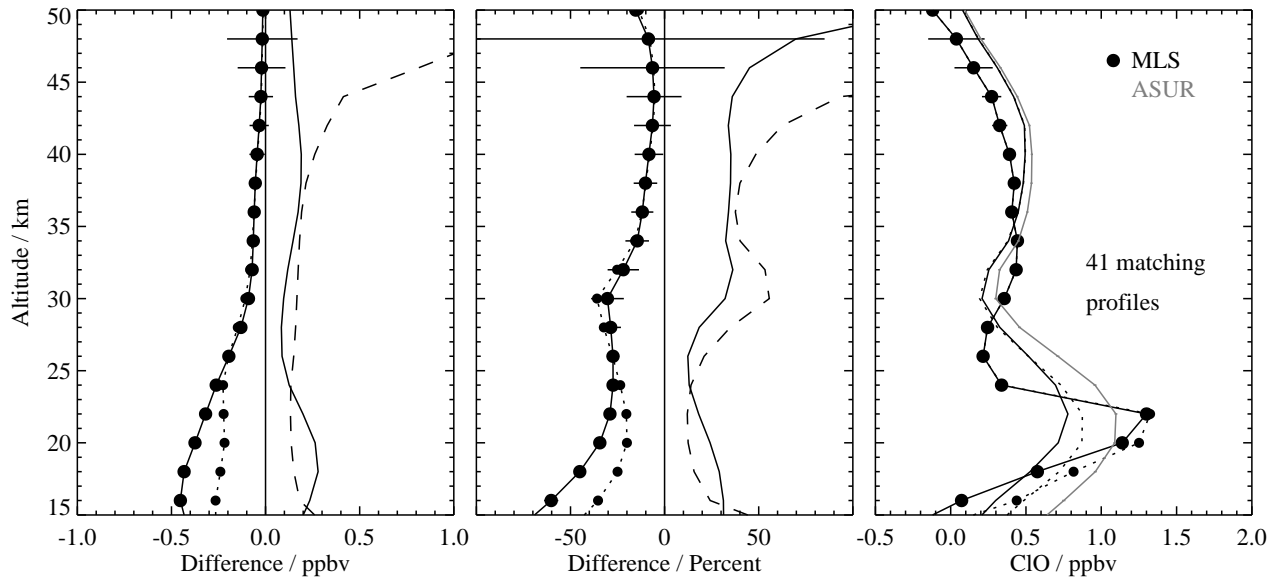


Figure 14. Summary of comparisons of coincident MLS v2.2 and ASUR CIO profiles. (Left) Absolute differences (MLS–ASUR, where the MLS data have been interpolated onto the ASUR grid and multiplied by the ASUR averaging kernels); the solid line with large dots shows mean differences with the “raw” MLS data, and the dotted line with small dots shows mean differences with the MLS data corrected for the negative bias as described in section 2.7. The solid line (with no symbols) shows the standard deviation about the mean differences, and the dashed line shows the root sum square of the theoretical precisions of the two datasets. (Middle) Same, for percent differences, where percentages have been calculated by dividing the mean differences by the mean ASUR values at each surface. (Right) Mean profiles for MLS (solid line with large dots for “raw” MLS data, dotted line with small dots for corrected MLS data), MLS multiplied by the ASUR averaging kernels (solid line with no symbols for “raw” MLS data, dotted line with no symbols for corrected MLS data), and ASUR (grey).

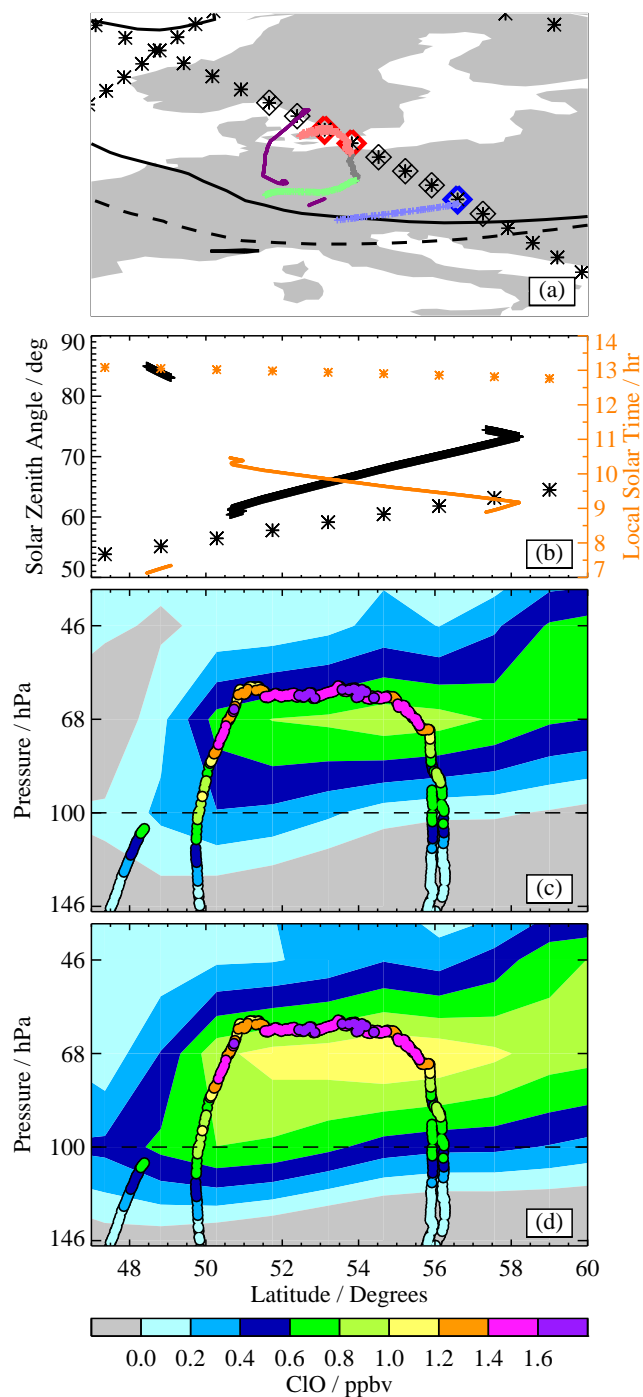


Figure 15. (a) Flight track (dark magenta) of the M55 Geophysica aircraft inside the Arctic polar vortex on 7 March 2005. Nearby MLS ground tracks on this day are denoted by asterisks; the specific MLS measurement points displayed in the contour plots of panels (c) and (d) are highlighted with diamonds, and the three MLS profiles shown in Figure 16 are outlined in blue and red. The position of the HALOX flight path shifted to the time of the MLS overpass using trajectory calculations based on European Centre for Medium-Range Weather Forecast (ECMWF) reanalyses are also shown, color-coded for different flight segments: ascent (pale blue), dive (pale red), level flight on return leg (grey) and descent (pale green). Overlaid in black are contours of GEOS-4 PV representative of the vortex edge at 410 K (solid line) and 460 K (dashed line), corresponding to the MLS retrieval levels at 100 and 68 hPa, respectively. (b) Solar zenith angle (large black symbols) and local solar time (small orange symbols) for the MLS (asterisks) and HALOX (plus signs) measurements. (c) V2.2 MLS CIO (contours) for the measurement points indicated in panel (a). The dashed line at 100 hPa signifies that the MLS data below this level are not considered reliable for scientific studies. Overlaid (filled circles) are the HALOX CIO measurements. (d) As in panel (c), but with the bias correction described in section 2.7 applied to the MLS CIO measurements.

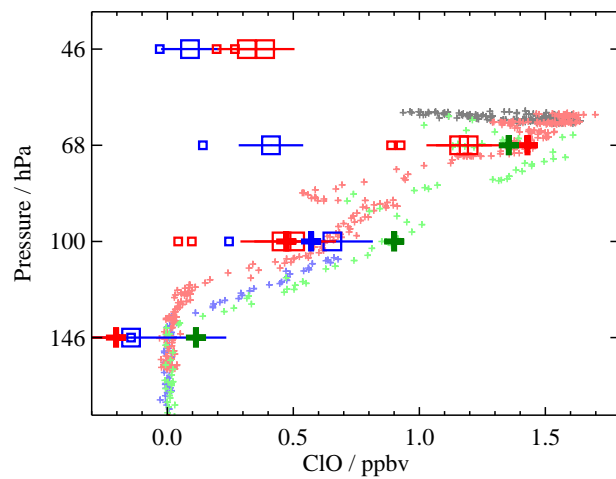


Figure 16. Three profiles of MLS CIO, color-coded as in Figure 15a, where small boxes show “raw” MLS values and large boxes show bias-corrected values (note that no bias correction is performed at 147 hPa, as the MLS CIO data are not deemed reliable for scientific use at this level). Error bars on corrected MLS points represent estimated precision. Also shown are HALOX measurements from the ascend, dive, level flight, and descend flight segments (small plus signs), color-coded as in Figure 15a, and the corresponding least-squares interpolation of the HALOX data multiplied by the MLS averaging kernels (see text; large plus signs in darker shades). Because of the shape of the MLS averaging kernel at 147 hPa (see Figure 3), to achieve proper smoothing at that level in situ data must be available up to at least 68 hPa; lack of high-altitude HALOX data during ascent (blue symbols) thus precludes conversion to the MLS grid at either 68 or 147 hPa.

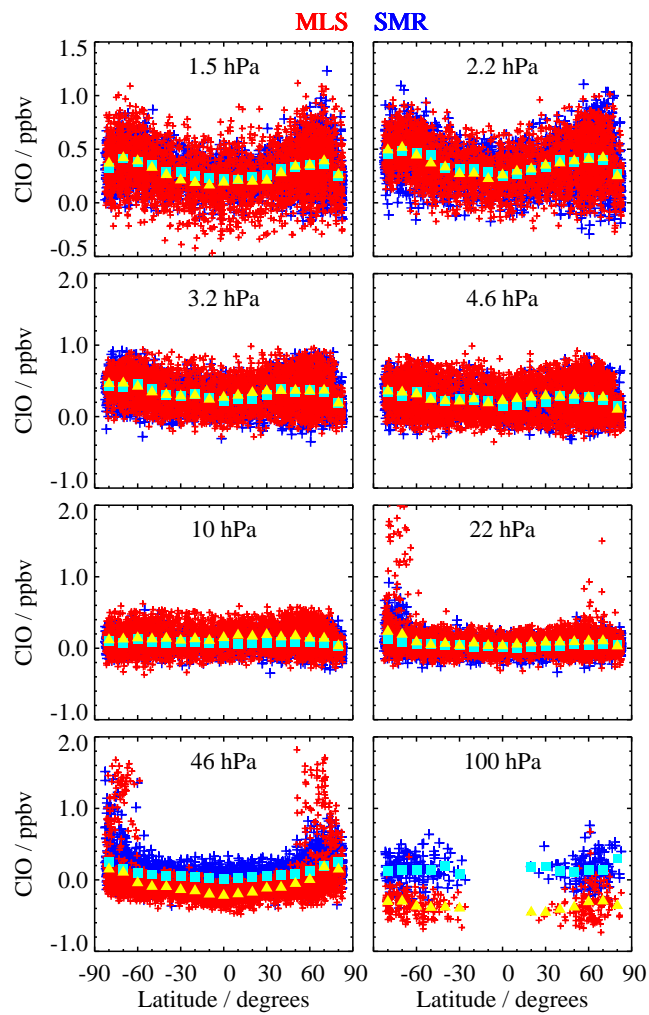


Figure 17. Scatter plot of coincident ClO profiles from MLS v2.2 data (red) and Odin/SMR Chalmers version 2.1 data (blue, see text), as a function of latitude for eight selected retrieval surfaces. Overplotted are the zonal-mean values calculated in 10°-wide latitude bands for both the MLS (yellow triangles) and SMR (cyan squares) data.

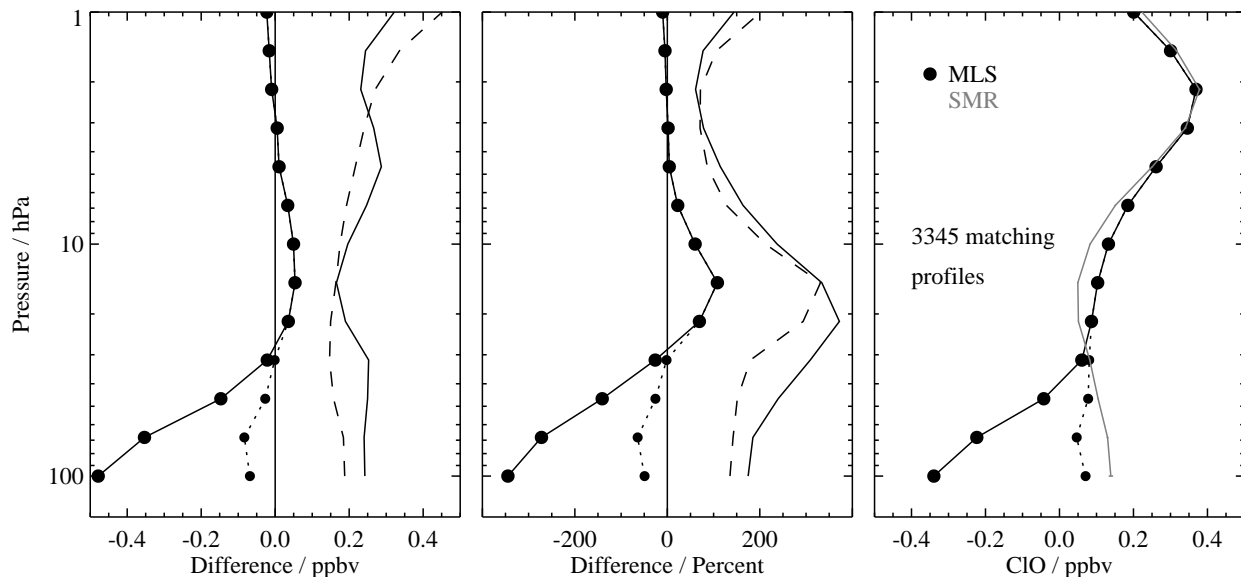


Figure 18. Comparison of coincident ClO profiles from MLS v2.2 data and Odin/SMR Chalmers version 2.1 data. (Left) Absolute differences (MLS–SMR); the solid line with large dots (symbols indicate MLS retrieval surfaces) shows mean differences with the “raw” MLS data, and the dotted line with small dots shows mean differences with the MLS data corrected for the negative bias as described in section 2.7. The solid line (with no symbols) shows the standard deviation about the mean differences, and the dashed line shows the root sum square of the theoretical precisions of the two datasets. (Middle) Same, for percent differences, where percentages have been calculated by dividing the mean differences by the global mean SMR value at each surface. (Right) Global mean profiles for MLS (solid line with large dots for “raw” MLS data, dotted line with small dots for corrected MLS data) and SMR (grey).

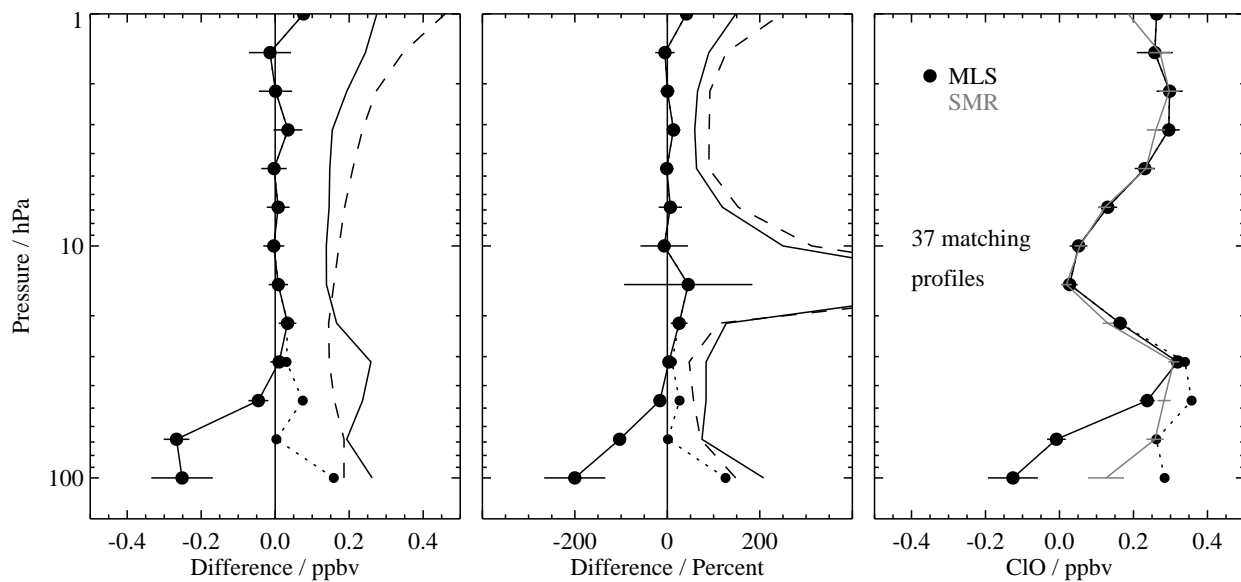


Figure 19. As in Figure 18, with additional SZA and LST coincidence criteria imposed (see text).

769 **Tables****Table 1.** Meaning of bits in the ‘Status’ field

Bit	Value ^a	Meaning
0	1	Flag: Do not use this profile (see bits 8–9 for details)
1	2	Flag: This profile is ‘suspect’ (see bits 4–6 for details)
2	4	Unused
3	8	Unused
4	16	Information: This profile may have been affected by high altitude clouds
5	32	Information: This profile may have been affected by low altitude clouds
6	64	Information: This profile did not use GEOS-5 temperature a priori data
7	128	Unused
8	256	Information: Retrieval diverged or too few radiances available for retrieval
9	512	Information: The task retrieving data for this profile crashed (typically a computer failure)

^a ‘Status’ field in L2GP file is the total of appropriate entries in this column.

Table 2. Summary of Aura MLS v2.2 CIO Characteristics

Pressure / hPa	Resolution		Bias	Scaling	Known Artifacts or Other Comments
	Vert. ×	Precision ^b	uncertainty ^c	uncertainty ^c	
	Horiz. ^a	/ ppbv	/ ppbv	/ %	
	/ km				
0.68–0.001	—	—	—	—	Unsuitable for scientific use
1.0	3.5 × 350	±0.3	±0.05	±15%	
22–1.5	3–4.5 × 250–400	±0.1	±0.05	±5–15%	
32	3 × 400	±0.1	±0.1	±10%	–0.02 ppbv systematic bias ^d
46	3 × 450	±0.1	±0.1	±20%	–0.12 ppbv systematic bias ^d
68	3 × 500	±0.1	±0.1	±20%	–0.27 ppbv systematic bias ^d
100	3.5 × 500	±0.1	±0.1	±20%	–0.41 ppbv systematic bias ^d
147–316	—	—	—	—	Unsuitable for scientific use
1000–464	—	—	—	—	Not retrieved

^a Horizontal resolution in along-track direction; cross-track resolution is ~ 3 km, and the separation between adjacent retrieved profiles along the measurement track is 1.5° great circle angle (~ 165 km).

^b Precision on individual profiles, determined from observed scatter in nighttime (descending) data in a region of minimal atmospheric variability.

^c Values should be interpreted as $2\text{-}\sigma$ estimates of the probable magnitude and, at the higher pressures, are the uncertainties after subtraction of the known negative bias tabulated in the rightmost column.

^d Determined directly from the observations, not from simulations. Values quoted are based on averages over middle and high latitudes; see section 2.7 for latitudinal variations in the magnitude of the bias estimates.